



Interactive Biogenic Emissions and Drought Stress Effects on Atmospheric Composition in NASA GISS ModelE

Elizabeth Klovenski¹, Yuxuan Wang¹, Susanne E. Bauer², Kostas Tsigaridis^{2,3}, Greg Faluvegi^{2,3}, Igor Aleinov^{2,3}, Nancy Y. Kiang², Alex Guenther⁴, Xiaoyan Jiang⁴, Wei Li¹, Nan Lin⁵

¹ Department of Earth and Atmospheric Sciences, University of Houston, Houston, TX, USA

² NASA Goddard Institute for Space Studies, New York, NY, USA

³ Center for Climate Systems Research, Columbia University, New York, NYC, USA

⁴ Department of Earth System Science, University of California – Irvine, Irvine, CA, USA

⁵ Ministry of Education Key Laboratory for Earth System Modeling, Department of Earth System Science, Tsinghua University, Beijing, China

Corresponding author: Yuxuan Wang (ywang246@central.uh.edu)

Key Points:

- A new method to capture regional changes of isoprene drought stress is implemented for global usage in NASA GISS ModelE and is evaluated at the MOFLUX Ameriflux site located in Missouri.
- The inclusion of isoprene drought stress from 2003-2013 leads to a ~2.7% reduction in global decadal average of isoprene emissions in ModelE with up to ~20% reduction in drought-stricken regions.
- The model-tuned parameterization of isoprene drought stress reduces the overestimation of ΩHCHO in the southeastern U.S and improves simulated O_3 during drought periods.

Abstract. Drought is a hydroclimatic extreme that causes perturbations to the terrestrial biosphere, and acts as a stressor on vegetation, affecting emissions patterns. During severe drought, isoprene emissions are reduced. In this paper, we focus on capturing this reduction signal by implementing a new percentile isoprene drought stress (y_d) algorithm in NASA GISS ModelE based on the MEGAN3 (Model of Emissions of Gases and Aerosols from Nature Version 3) approach as a function of a photosynthetic parameter ($V_{c,max}$) and water stress (β). Four global transient simulations from 2003-2013 are used to demonstrate the effect without y_d (Default_ModelE) and with online y_d (DroughtStress_ModelE). DroughtStress_ModelE is evaluated against the observed isoprene measurements at the Missouri Ozarks Ameriflux (MOFLUX) site during the 2012 severe drought where improvements in correlation coefficient indicate it is a suitable drought stress parameterization to capture the reduction signal during severe drought. The application of y_d globally leads to a decadal average reduction of ~2.7% which is equivalent to ~14.6 Tg yr⁻¹ of isoprene. The changes have larger impacts in regions such as the Southeast U.S.. DroughtStress_ModelE is validated using satellite ΩHCHO column from the Ozone Monitoring Instrument (OMI) and surface O_3 observations across regions of the U.S. to examine the effect of drought on atmospheric composition. It was found the inclusion of isoprene drought stress reduced the overestimation of ΩHCHO in Default_ModelE during the



2007 and 2011 southeastern U.S. droughts and lead to improvements in simulated O_3 during drought periods. We conclude that isoprene drought stress should be tuned on a model-by-model basis, because the variables used in the parameterization responses are relative to the land surface model hydrology scheme (LSM) and the effects of y_d application could be larger than seen here due to ModelE not having large biases of isoprene during severe drought.

Plain Language Summary: Severe drought stresses vegetation and causes reduced emission of isoprene. We study the impact of including a new isoprene drought stress (y_d) parameterization into NASA GISS ModelE called (DroughtStress_ModelE), which is specifically tuned for ModelE. Inclusion of y_d leads to better simulated isoprene emissions at the MOFLUX site during the severe drought of 2012, reduced overestimation of OMI satellite $\Omega HCHO$ (formaldehyde column) and improved simulated O_3 (ozone) during drought.

1. Introduction

In present day conditions terrestrial ecosystems release about $1000 \text{ Tg C yr}^{-1}$ of biogenic volatile organic compounds (BVOCs) into the atmosphere and there is an additional smaller emission from marine ecosystems (Guenther *et al.* 2012). The majority of BVOCs emitted from vegetation are isoprene and monoterpenes (Guenther *et al.* 2006; Guenther *et al.* 2012). Representing over half of emitted BVOCs, isoprene is the dominant species globally with reported ranges of $440\text{--}600 \text{ Tg C yr}^{-1}$ (Guenther *et al.* 2012) with high emission factors from some, but not all, broadleaf trees including species of oak, willow, palm oil, and eucalyptus (Benjamin *et al.* 1996; Geron *et al.* 2000). Isoprene is produced from carbon substrates generated during photosynthesis and contributes to abiotic stress tolerance from water and temperature stress (Loreto and Sharkey 1990; Monson *et al.* 2021). Isoprene emissions peak during warm, sunnier months of the growing season (MAR-OCT) (Opacka *et al.* 2021). Isoprene has a chemical lifetime of approximately one hour via oxidation by the hydroxyl radical (OH), producing organic aerosols and oxidation products that contribute to ozone (O_3) formation (Carlton *et al.* 2009). Biogenic isoprene emissions affect atmospheric composition and climate, and in turn depend on drivers including light, temperature, photosynthetically active radiation (PAR), leaf area index (LAI), water stress, ambient O_3 , and CO_2 concentrations. Climate change-related higher temperatures and CO_2 concentrations are separately expected to increase emissions of BVOCs, which will impact tropospheric ozone and secondary organic aerosols (SOA) formation. Increasing SOA will have a negative climate forcing effect through increased scattering of sunlight, causing an aerosol direct forcing, and increased cloud condensation nuclei (CCN), causing aerosol indirect forcing effects (Twomey 1974; Sporre *et al.* 2019). The consideration of drought effects on BVOC emissions, as investigated in this study, will counterbalance these effects, due to isoprene reductions caused by drought stress. During drought, increases in SOA and O_3 are to be expected (Wang *et al.* 2017; Zhao *et al.* 2019), and with isoprene reductions we expect a reduction in the magnitude of increase of both pollutants. SOA acts as negative radiative forcing under future temperature and CO_2 increases (Zhu *et al.* 2017) and tropospheric O_3 and total O_3 acts as a positive radiative forcing (Skeie *et al.* 2020).



85

86 Drought is a common abiotic stress to terrestrial ecosystems characterized by low soil
87 moisture, usually associated with high temperature and low precipitation. However, even boreal
88 forests undergo winter drought due to frozen soils. Recent work has shown a strong correlation
89 between drought severity and fine-mode aerosols in the U.S. and estimated that regions
90 undergoing severe drought see up to 17% surface enhancement of aerosols during the growing
91 season (Wang *et al.* 2017). This suggests a strong perturbation of drought to atmospheric
92 aerosols, likely caused by changing BVOC emissions due to drought stress. Limited field and lab
93 measurements have shown that during drought, isoprene has a unique emission response where
94 initial increase in temperature causes an increase in emission, but prolonged or severe drought
95 causes a decrease of emissions due to the shutdown of physiological processes (Potosnak *et al.*
96 2014). This behavior is not reproduced by commonly used BVOC emission models such as the
97 Model of Emissions of Gases and Aerosols from Nature Version 2.1 (MEGAN2.1), which has a
98 simple drought algorithm which is often not used due to the unavailability of the required driving
99 variables in chemistry climate models (CCMs), and the Biogenic Emission Inventory System
100 (BEIS), which does not include a drought algorithm as an option.

101

102 Isoprene flux observations at the Missouri Ozarks (MOFLUX) Ameriflux site in Missouri (SI
103 Fig. S1) recorded a moderate drought in summer 2011 (Potosnak *et al.* 2014) and a particularly
104 severe drought event in summer 2012 (Seco *et al.* 2015). To the best of our knowledge, these are
105 the only in situ isoprene flux measurements capturing a drought anywhere. Using the MOFLUX
106 observations, Jiang *et al.* (2018) developed an isoprene drought stress activity factor for
107 MEGAN3 (Model of Emissions of Gases and Aerosols from Nature Version 3) designed to
108 reduce emissions of isoprene during drought. The previous MEGAN2.1 isoprene drought
109 parameterization utilized soil moisture and soil wilting point threshold to include impacts of
110 drought on photosynthetic processes. The MEGAN3 isoprene drought stress activity factor is a
111 more process-based parameterization based on a photosynthetic parameter ($V_{c,max}$) and water
112 stress (β) from the Community Land Model (CLM) as coupled with the CAM-Chem climate
113 model (Jiang *et al.* 2018). $V_{c,max}$ is the maximum carboxylation capacity of a leaf (usually in units
114 of micromole CO₂ per leaf area per time); that is, it is the ability of a plant to convert CO₂ into
115 sugar, and hence determine productivity of carbon substrates for biogenic volatile organic
116 compounds (BVOCs) production when no other conditions are limiting. β is a scaling factor
117 between zero to one, used in CLM to reduce $V_{c,max}$ due to plant water stress. MEGAN3 isoprene
118 drought stress was also incorporated into the CSIRO chemical transport model (C-CTM) with
119 Australian land surface models Mk3.6 Global Climate Model and the Soil-Litter-Iso model with
120 a focus on Australia (Emmerson *et al.* 2019). Both prior modeling studies (Jiang *et al.* 2018;
121 Emmerson *et al.* 2019) only looked at the drought effects on O₃; here we study the combined
122 effect of drought on O₃ and formaldehyde column.

123



The accurate simulation of stress-affected emissions of isoprene during extreme hydroclimate events (i.e. drought) is crucial to understanding vegetation-climate-chemistry feedbacks, because isoprene is a precursor to tropospheric O₃ and SOA, both being climate forcers as well as air pollutants. Here we focus on deriving a model-specific tuned isoprene drought stress factor that is coupled into the existing MEGAN2.1 framework in NASA GISS ModelE, an Earth System Model, to model the effect of drought on isoprene emissions and their effect on atmospheric composition. The model-specific tuning is required due to different land system models parameterizing key variables of $V_{c,max}$ and β in different ways with varying distributions. The model's drought effects will be extensively evaluated over the US, due to the availability of observational evidence during drought (Wang *et al.* 2017). While the MOFLUX data are the only available measurements of isoprene emissions during drought, formaldehyde (HCHO), the high yield oxidation product of isoprene, can be used as a proxy for isoprene emissions (Zhu *et al.* 2016). **Section 2** describes the modelling approaches used to represent drought impacts on isoprene emissions. **Section 3** describes the comparison of modeled isoprene emissions to observations at the MOFLUX site during drought along with necessity of building a model specific isoprene drought stress parameterization. **Section 4** details the comparisons between simulation with model specific tuned isoprene drought stress (DroughtStress_ModelE) and observational O₃, PM_{2.5} (particulate matter $\leq 2.5 \mu\text{m}$), and tropospheric formaldehyde columns (QHCHO) over North America.

143

144 2. Methods and Data

145 2.1. The biogenic emission model MEGAN

MEGAN is a widely used BVOC emissions model that is implemented in many CCMs. Here we describe briefly MEGAN2.1 as implemented in ModelE. MEGAN2.1 calculates the net primary emissions for 20 compound classes, which are speciated into over 150 species such as isoprene, monoterpenes, etc. (Guenther *et al.* 2012). The emissions rate ($\mu\text{g grid cell}^{-1} \text{h}^{-1}$) of each compound into the above canopy atmosphere from a model grid cell is calculated:

151

$$152 \text{ Emission} = EF \times y \times S \quad (1)$$

153

where EF ($\mu\text{g m}^{-2} \text{h}^{-1}$) is emission factor per compound, y is the dimensionless emission activity factor that accounts for emission response to phenological and meteorological conditions, and S is the grid cell area (m^2).

157

The emission activity factor y for each compound is calculated following the MEGAN2.1 parameterization (Guenther *et al.* 2006; Guenther *et al.* 2012; Henrot *et al.* 2017).

160

$$161 y = y_{CE} \times y_A \times y_d \times y_{Co_2} \quad (2)$$

162



Where y_{CE} is the canopy environment coefficient, assigned a value of one for standard conditions, and it takes into account variations associated with LAI ($\text{m}^2 \text{m}^{-2}$), photosynthetic photon flux density (PPFD) (μmol of photons in 400-700 nm range $\text{m}^{-2} \text{s}^{-1}$), and temperature (K). y_A is the leaf age emission activity factor, parameterization of which is based on coefficients of the decomposition of the canopy into new, growing, mature, and senescing leaves for current and previous months' LAI (Guenther *et al.* 2006; Guenther *et al.* 2012). y_d is the isoprene drought stress activity factor and y_{CO_2} is the isoprene emission activity factor associated with CO_2 inhibition (for all other compounds y_d and $y_{CO_2} = 1$). The biogenic emission module implemented in ModelE follows the ECHAM6-HAMMOZ online MEGAN2.1 implementation (Henrot *et al.* 2017) in a CCM. Within ModelE the MEGAN2.1 module maps the 16 plant functional types (PFTs) from Ent TBM (Terrestrial Biosphere Model) (Kim *et al.* 2015) into 16 MEGAN PFTs, and contains 13 chemical compound classes. ModelE uses a modified MEGAN2.1 following (Henrot *et al.* 2017) to provide a framework to simulate isoprene emissions, and uses prescribed emissions factors per PFT to simulate emissions per compound class.

In Henrot *et al.* (2017) to avoid using a detailed canopy environment model calculating light and temperature at each canopy depth, the Parameterized Canopy Environmental Emission Activity (PCEEA) approach from Guenther *et al.* (2006) is used to replace y_{CE} with a parameterized canopy environment activity factor ($y_{LAI} \times y_P \times y_T$). With this approach the light dependent and light independent factors are multiplied by y_{LAI} not LAI so they are not directly proportional to LAI. This approach allows for calculation of light dependent emissions following isoprene emission response to temperature, where its assumed the light dependent factor (LDF) equals one for isoprene and light independent emissions follow the monoterpene exponential temperature response. Please see Guenther *et al.* (2006); Guenther *et al.* (2012); Henrot *et al.* (2017) for activity factor parameterizations. At any given time step in ModelE, the emissions formula for a compound class (c) and PFT (i), in units of $\text{kg m}^{-2} \text{s}^{-1}$ is given by:

$$Emission_{i,c} = (1 \times 10^{-9} / 3600) \times (EF_{i,c} \times PFTboxf_i) \times y_{LAI} \times y_A \times y_d \times y_{CO_2} \times ((1 - LDF) \times y_{TLI} + LDF \times y_P \times y_{TLD}) \times SF_c \times MWC_c \quad (3)$$

where $EF_{i,c}$ is the emissions factor ($\mu\text{g m}^{-2} \text{hr}^{-1}$) for a given PFT and compound class, $PFTboxf_i$ is the fraction of the grid cell (ranging from zero to one) covered by PFT i , and SF_c is a linear scale factor for compound class c . The activity factors, y , listed in Equation (3) are unitless and account for the emissions response to leaf area index (LAI), aging (A), drought (d), CO_2 (CO_2), and PPFD (P). The LDF, weights the contributions from light independent (y_{TLI}) and light dependent (y_{TLD}) emissions response to temperature. MWC_c stands for a molecular weight conversion to remove non-carbon mass, if appropriate. ($1 \times 10^{-9} / 3600$) is a timestep conversion for seconds in an hour. Note that although the drought activity factor y_d is present in ModelE, it is set to equal one in all cases prior to this work, meaning no drought effects on BVOC emissions in the model.



For example, the emission formula for the compound class of isoprene in ModelE for PFT i is as follows (where LDF=1):

$$Isoprene_i = (1 \times 10^{-9} / 3600) \times (EF_{i, isoprene} \times PFTboxf_i) \times y_{LAI} \times y_A \times y_d \times y_{CO_2} \times (y_P \times y_{TLD}) \times SF_{isoprene} \times (60.05 / 68.12) \quad (4)$$

2.2 MEGAN2.1 Isoprene Drought Stress Emission Algorithm

Guenther *et al.* (2006) introduced isoprene drought stress as a soil moisture dependent algorithm called y_{SM} . This isoprene drought stress activity factor relied upon soil moisture and wilting point to apply drought stress to isoprene emissions. The algorithm for soil moisture isoprene drought stress is as follows:

$$y_{SM} = 1 \text{ when } \theta > \theta_1 \quad (5a)$$

$$y_{SM} = \frac{\theta - \theta_w}{\Delta\theta_1} \text{ when } \theta_w < \theta < \theta_1 \quad (5b)$$

$$y_{SM} = 0 \text{ when } \theta < \theta_w \quad (5c)$$

where θ is soil moisture (volumetric water content $m^3 m^{-3}$), θ_w is the point beyond which plants cannot extract water from soil, known as the wilting point, $m^3 m^{-3}$, $\Delta\theta_1$ ($=0.06$ in Guenther *et al.* 2006 and $=0.04$ in Guenther *et al.* 2012) is an empirical parameter, and θ_1 is defined as $\theta_w + \Delta\theta_1$. Soil moisture and wilting point are not widely available parameters in models, and y_{SM} was not widely adopted to represent isoprene drought stress as studies showed substantial uncertainty associated with soil moisture predicted response of isoprene emission to water stress and in selection of wilting point values (Müller *et al.* 2008; Tawfik *et al.* 2012; Sindelarova *et al.* 2014; Huang *et al.* 2015; Jiang *et al.* 2018). There also exist challenges associated with validating soil moisture datasets due to the limited spatial coverage of in-situ root-zone measurements in the contiguous United States (Ochsner *et al.* 2013). A study found that the accurate simulation of soil moisture in land surface models was highly model-dependent, due to the differing horizontal and vertical spatial resolution of such models at large scales (Koster *et al.* 2009). Potosnak *et al.* (2014) determined that the selection of different wilting point values greatly impacted the drought impacts on biogenic isoprene emission. With these associated challenges, it was rare to find isoprene drought stress implemented in CCMs, thus a new isoprene drought activity factor needed to be developed that could be easily incorporated into a variety of models that had a land surface model (LSM) or terrestrial biosphere model (TBM).

2.3 MEGAN3 Isoprene Drought Stress Emission Algorithm

Jiang *et al.* (2018) developed a new isoprene drought stress activity factor in MEGAN3 that focuses on photosynthetic carboxylation capacity and water stress to model reductions of vegetative isoprene during drought. The algorithm was developed using isoprene flux observations during the severe drought of the summer of 2012 and less severe drought of 2011 (Potosnak *et al.* 2014; Seco *et al.* 2015) at MOFLUX. The MOFLUX site is located in the University of Missouri Baskett Wildlife Research area in central Missouri which is known as the isoprene volcano (Wells *et al.* 2020). The MOFLUX site is comprised primarily of deciduous



broadleaf trees, primarily oaks, known to emit high quantities of isoprene. All meteorological data from the site comes from the Ameriflux website (<https://ameriflux.lbl.gov/sites/siteinfo/US-MOz#overview>).

We refer to the original MEGAN3 drought stress developed by Jiang *et al.* (2018) to be **DroughtStress_MEGAN3_Jiang**, and the corresponding parameterization for isoprene activity factor during drought where (y_d) is a function of PFT and where the values of $V_{c,max}$ and β are specified by PFT is:

$$y_d = 1, \text{ when } \beta \geq 0.6 \quad (6a)$$

$$y_d = \frac{(V_{c,max} \times \beta)}{\alpha}, \text{ when } \beta < 0.6, \alpha = 37 \quad (6b)$$

$$0 \leq y_d \leq 1 \quad (6c)$$

$$Isoprene_i = (1 \times 10^{-9} / 3600) \times (EF_{i,isoprene} \times PFTboxf_i) \times y_{LAI} \times y_A \times y_d \times y_{CO_2} \times (y_P \times y_{TLD}) \times SF_{isoprene} \quad (7)$$

The drought stress activity factor, y_d , in **DroughtStress_MEGAN3_Jiang** was originally developed using the Community Land Model Version 4.5 (CLM4.5) (Jiang *et al.* 2018). The photosynthetic parameter used is $V_{c,max}$, which is the maximum rate of leaf-level carboxylation. In ModelE, $V_{c,max}$ is scaled with an enzymatic kinetics response to temperature, and drought stress reduces leaf stomatal conductance, thereby reducing photosynthetic activity through CO_2 diffusion limitation rather than by reduction of $V_{c,max}$. In CLM4.5, $V_{c,max}$ is a function of nitrogen (Jiang *et al.* 2018). Water stress in CLM4.5 is based on soil texture (Clapp and Hornberger 1978), and it is a function of soil water potential of each soil layer, wilting factor, and PFT root distribution. Water stress (β) ranges from zero when a plant is completely stressed to one when a plant is not undergoing stress. In CLM4.5, $V_{c,max}$ is scaled online by β before being applied into the isoprene drought activity parameterization, thus this scaling step is not reflected in the equations shown by Jiang *et al.* (2018). Since ModelE does not scale $V_{c,max}$ by β (instead, ModelE scales leaf stomatal conductance by β), to reproduce the original scheme by Jiang *et al.* (2018) as much as possible in ModelE, we scaled $V_{c,max}$ with β inside the equation of isoprene drought activity factor as in Eq. (6b). y_d as defined in Eq. (6) is then applied in ModelE as an activity factor into the MEGAN2.1 isoprene emissions equation per every plant functional type (PFT) and the modeling results from this simulation are referred to as **DroughtStress_MEGAN3_Jiang**. The y_d ranges from zero to one and is designed to reduce isoprene emissions during severe and prolonged drought.

2.4 NASA GISS ModelE Climate Chemistry Model

NASA GISS ModelE2.1 is an Earth System Model (ESM) with a horizontal and vertical resolution of 2° degrees in latitude and 2.5° degrees in longitude with 40 vertical layers from the surface to 0.1 hPa (Kelley *et al.* 2020). The climate model is configured in CMIP6 (Coupled



Model Intercomparison Project Phase 6) configuration (Miller *et al.* 2021) with fully coupled atmospheric composition with interactive gas-phase chemistry. The model described here is driven by historical Atmospheric Model Intercomparison Project simulations (AMIP), using prescribed ocean temperature and sea ice datasets. There are two aerosol schemes to choose from: MATRIX (“Multiconfiguration Aerosol TRacker of mIXing state”) (Bauer *et al.* 2008) a microphysical aerosol scheme and OMA (One-Moment Aerosol) mass-based aerosol scheme (Koch *et al.* 2006; Miller *et al.* 2006; Bauer *et al.* 2007; Tsigaridis *et al.* 2013; Bauer *et al.* 2020). Here we use the OMA scheme, due to its better representation of secondary organic aerosol chemistry (Tsigaridis *et al.* 2013). SOA is calculated using the CBM4 chemical mechanism to describe the gas phase tropospheric chemistry together with all main aerosol components including SOA formation and nitrate, and is calculated using four tracers in the model. Isoprene (VOCs) contribute to the formation of SOA. OMA has 34 tracers for the representation of aerosols that are externally mixed, except for mineral dust that can be coated (Bauer *et al.* 2007), and has prescribed constant size distribution (Bauer *et al.* 2020). OMA aerosol schemes are coupled to the stratospheric and tropospheric chemistry scheme (Shindell *et al.* 2013) which includes inorganic chemistry of O_x , NO_x , HO_x , CO, and organic chemistry of CH_4 and higher hydrocarbons, with explicit treatment of secondary OA (organic aerosol), and the stratospheric chemistry scheme which includes chlorine and bromine chemistry together with polar stratospheric clouds. O_3 and aerosols impact climate via coupling to the radiation scheme, and aerosols serve as cloud condensation nuclei (CCN) for cloud activation. The model includes the first indirect effect. Sea salt, dimethyl sulfide (DMS), and biogenic dust emission fluxes are calculated interactively, while anthropogenic dust is not represented in ModelE2.1. Other anthropogenic fluxes are from the Community Emissions Data System Inventory (CEDS) (Hoesly *et al.* 2018) and biomass burning is from GFED4s (Global Fire Emissions Database with small fires) inventory (van Marle *et al.* 2017) for 1850-2014.

Vegetation activity in ModelE is simulated with a dynamic global vegetation model, the Ent Terrestrial Biosphere Model (Ent TBM) (Kim *et al.* 2015). In standard ModelE experiments, the Ent TBM prescribes satellite-derived vegetation canopy structure (plant functional type, canopy height, monthly leaf area index) (Ito *et al.* 2020) as boundary conditions for coupling the biophysics of canopy radiative transfer, photosynthesis, vegetation and soil respiration, and transpiration with the land surface model and atmospheric model. These processes provide surface fluxes of CO_2 and water vapor, and surface albedo is specified by cover type and season. ModelE uses the MEGAN2.1 BVOC emissions model to simulate interactive biogenic emissions from vegetation (Guenther *et al.* 2006; Guenther *et al.* 2012). Ent TBM water stress is calculated as a scaling factor between zero and one as a function of relative extractable water (REW) for the given soil texture and PFT-dependent levels of REW for onset of stress and wilting (Kim *et al.* 2015); this scaling has been updated since Kim *et al.* (2015) to be a function of the water stress factor of only the wettest soil layer in the PFT’s root zone. Ent TBM uses a leaf-level model of coupled Farquhar-von Caemmerer photosynthesis/Ball-Berry stomatal conductance (Farquhar



and von Caemmerer 1982; Ball and Berry 1985). The model calculates an unstressed leaf photosynthesis rate and stomatal conductance, then applies its water stress scaling factor to scale down leaf stomatal conductance, to emulate how hormonal signaling by roots under water stress induces stomatal closure. Since there is a coupling of transpiration and CO₂ uptake through stomatal conductance, water stress thereby also reduces photosynthesis rate through the limitation on CO₂ diffusion into the leaf; this is different from CLM4.5's approach, which instead reduces $V_{c,max}$. Canopy radiative transfer in the Ent TBM scales leaf processes to the canopy scale by calculating the vertical layering of incident photosynthetically active radiation on sunlit versus shaded leaves. The different PFTs in Ent TBM have different critical soil moisture values for the onset of stress (when stomatal closure begins in response to drying soils) and their wilting point (when the plant is unable to withdraw moisture from the soil and complete stomatal closure occurs). It should be noted that the GISS land surface model is wetter than observed soil moisture (Kim *et al.* 2015). $V_{c,max}$ is a function of a Q₁₀ temperature function in ModelE. Since nitrogen dynamics are not represented yet in the Ent TBM, leaf nitrogen is fixed and therefore $V_{c,max}$ is not dynamic with nitrogen as in CLM4.5. The Q₁₀ coefficient is often used to predict the impact of temperature increases on the rate of metabolic change (Rasmusson *et al.* 2019).

To emulate the MEGAN/CLM representation of drought stress, in this study, in the Ent TBM leaf model, we applied a reduction in $V_{c,max}$ with water stress as shown in Eq. (6b). It is important to note that the reduction of $V_{c,max}$ with water stress in Eq. (6b), is not used outside the isoprene drought stress parameterization, so the $V_{c,max}$ reduction is not applied to the calculation of photosynthetic CO₂ uptake; this avoids applying another secondary indirect scaling to conductance, since the Ent TBM already applies its water stress factor to reduce stomatal conductance.

For this study, ModelE2.1 was configured with a transient atmosphere and ocean using a prescribed sea surface temperature (SST) and sea ice (SSI) according to observations. The transient simulations contain continuously-varying greenhouse gases in order to represent a realistic mode in present day. To facilitate direct comparison with atmospheric composition observations as in this study, meteorology is nudged to the National Centers for Environmental Prediction (NCEP) reanalysis winds. Four transient ModelE simulations were run for the period of 2003-2013 with a three-year spin-up using MEGAN2.1 with varying configurations for isoprene drought stress to be described below. The authors found that the default MEGAN implementation in ModelE2.1 underestimates isoprene and monoterpene emissions, thus appropriate scaling factors (SF_c) were applied to match literature for global annual emission estimates, 1.8 for isoprene and 3 for monoterpenes to match literature estimates of around ~500 Tg C of isoprene and ~130 Tg C of monoterpenes (Arneth *et al.* 2008; Guenther *et al.* 2012).

2.5 Observations of Isoprene Emissions at MOFLUX during Drought of 2011-2012



366 The MOFLUX site located at 38.7441°N, -92.2000°W (latitude, longitude) is comprised
 367 mostly of deciduous broadleaf forests dominated by oak-hickory forest and the climate is
 368 classified as humid subtropical with no dry season and hot summers. The site experienced a mild
 369 drought in the mid to late summer of 2011 and an extreme to exceptional drought from the mid
 370 to late summer of 2012 when concurrent biogenic isoprene flux measurements were taken. The
 371 2011 drought was not as severe as the drought of summer of 2012. The ecosystem response of
 372 isoprene has two stages including a mild phase of drought stress where emissions are stimulated
 373 by increases in leaf temperature due to reduced stomatal conductance while in the second stage
 374 of drought, the more severe phase of drought stress, emissions are suppressed by reduction in
 375 substrate availability or isoprene synthase production (Potosnak *et al.* 2014; Seco *et al.* 2015).

377 In 2011, the spring was wet but the drought started to appear in June due to lack of rainfall
 378 while temperatures broke records and continued through July (Potosnak *et al.* 2014; Jiang *et al.*
 379 2018). However, the USDM (U.S. Drought Monitor) did not capture this drought signal from
 380 June - July and only showed abnormally dry periods from August 2 - August 16, and never went
 381 into extreme (D2) or severe drought stage (D3). This suggests 2011 summer was a useful case
 382 only for studying drought response of isoprene during weak drought conditions. The highest
 383 observed isoprene fluxes were from July 11 – August 3 shown in Fig. 1a. Potosnak *et al.* (2014)
 384 reported that from July 14 - August 10 their MEGAN2.1 simulations consistently underestimated
 385 isoprene emissions during onset of drought and overestimated as drought progressed from
 386 August 18 to September 2. From August 3 – August 23 there was a total of 65 mm of
 387 precipitation, which led to an increase in observed soil moisture. It was suggested that since
 388 observed soil moisture increases during the period of drought progression when isoprene is
 389 decreasing (August 18 - September 2) relative to the onset of drought (July 14 - August 10), this
 390 indicates the response to drought stress during this year is time dependent, and a time-
 391 independent algorithm based on soil moisture will not capture the relevant processes during a
 392 less severe drought year. It was also noted that MEGAN2.1 underpredicts during the cooler
 393 months of May-June and underpredicts during the warmer month of July (Potosnak *et al.* 2014),
 394 and only overpredicts during small portions of August-September as denoted by a grey box in
 395 Fig. 1a. With this pattern of underprediction observed in MEGAN2.1 simulations and also seen
 396 in Default_ModelE, as well as weak drought conditions as stated above, 2011 is not an ideal year
 397 to tune an isoprene drought stress algorithm to target the reduction period caused by drought
 398 stress.

400 In 2012, there were three unique periods that displayed the development of a severe drought
 401 that make it ideal to tune an isoprene drought stress algorithm. Shown in Fig. 1b is the daily
 402 averaged isoprene flux broken up into three periods. We define the MAXVOC episode from
 403 May 1 - July 16, severe drought period (July 17-August 31) shaded in brown in Fig. 1b, and the
 404 drought recovery period (September 1-31). Although Seco *et al.* (2015) defined MAXVOC from
 405 June 18 – July 31, they identified July 16 as the transitional stage between MAXVOC episode



406 and severe drought. Thus, our work used July 16 to separate MAXVOC and severe drought
407 periods. The periods of pre-drought (prior to May 31) and mild drought identified by Seco *et al.*
408 (2015) from May 31- June 14 are included in the MAXVOC period, because during this time
409 period a typical seasonal pattern of increasing emissions with increasing temperatures is shown,
410 and there is no indication of decreasing emissions due to drought stress. The mild drought period
411 (May 31- June 14) corresponds to USDM periods of abnormally dry and moderate drought.
412 Isoprene emissions continue to increase during the beginning of summer, which is supported by
413 several studies that show isoprene emissions during the first stages of drought increase even
414 though there is a decrease in CO₂ fixation, which is attributed to drought induced stomatal
415 closure and rising leaf temperature and decreasing transpirational cooling and CO₂ concentration
416 in the leaf (Rosenstiel *et al.* 2003; Pegoraro *et al.* 2004; Potosnak *et al.* 2014; Seco *et al.* 2015).
417 Separating MAXVOC and severe drought period allows for the algorithm development to target
418 the latter severe drought stage where isoprene reduction occurs, while not reducing emissions
419 during the early, and less severe, stages of drought. During the severe drought period, total
420 annual precipitation was the lowest in a decade while soil water content reached its minimum at
421 the end of August when the drought peaked (Jiang *et al.* 2018). During the severe drought there
422 is a marked decrease in isoprene flux shown by the brown shaded box coinciding with lower β
423 values. It is well established that isoprene emissions are linked to high temperatures (Singsaas
424 and Sharkey 2000), and without the contributing factor of drought there should be a rising
425 increase in isoprene emissions in July and August. The severe drought period encompasses
426 periods of severe and extreme drought identified by the USDM. July 3 marks the first week
427 indicated by USDM of severe drought and July 31 marks the first week of extreme drought.
428 During severe drought isoprene production is suppressed by reductions in substrate availability
429 and isoprene synthase transcription (Potosnak *et al.* 2014). Rain events at the end of August led
430 to drought recovery and soil water content started to increase, which is indicated by increasing β
431 values shown in the drought recovery period indicated in purple in Fig. 1b. Overall, 2012 shows
432 a complete development of drought conditions that affect isoprene emissions and will provide
433 useful constraints on the drought stress factor parameterization: a MAXVOC period that
434 encompasses pre- and mild drought periods, a severe drought period (July 17 – August 31), and a
435 drought recovery period (September 1-30).



436

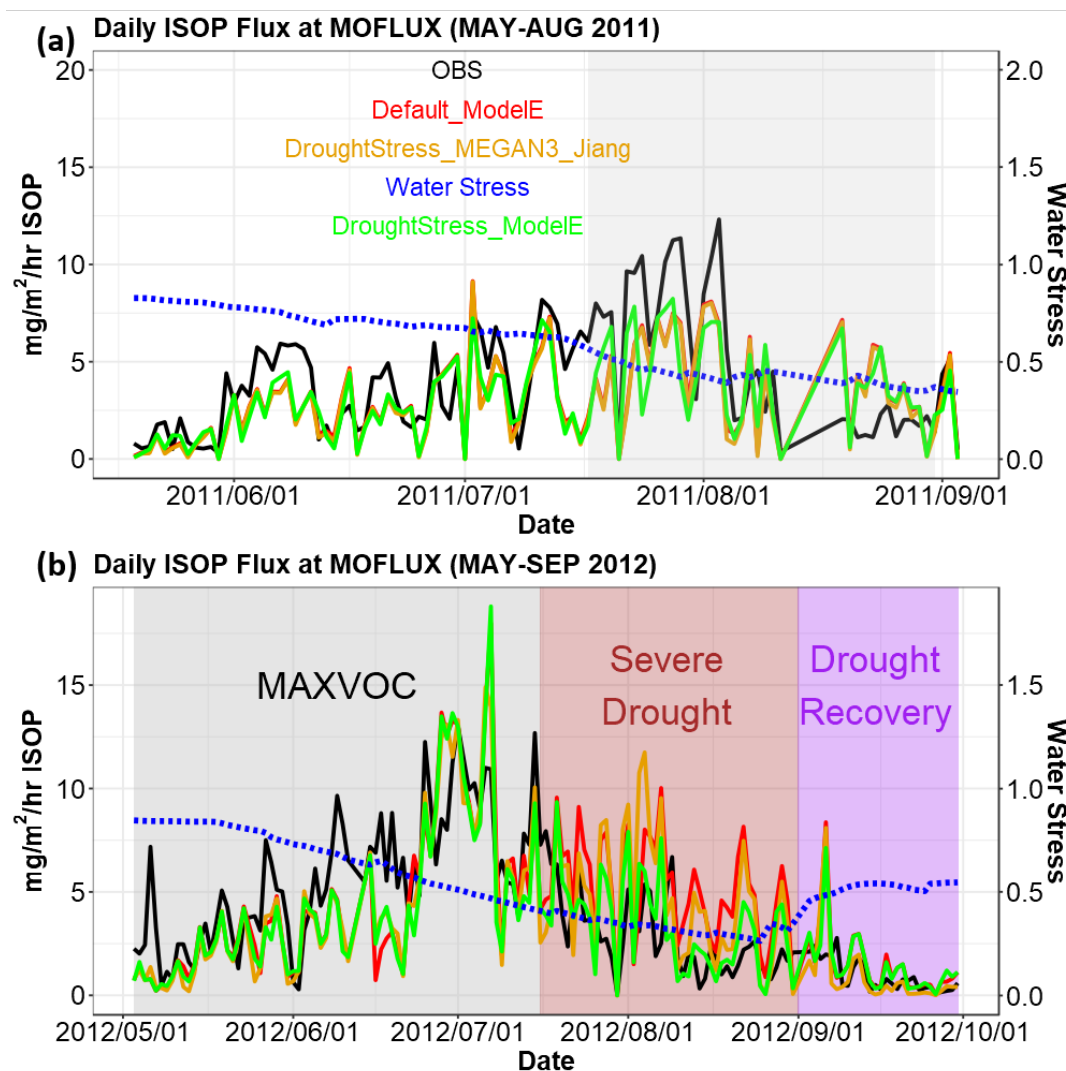


Figure 1. Daily isoprene emissions flux at MOFLUX (MAY-AUG 2011 and MAY-SEP 2012) LST timeseries are shown. Black shows observed isoprene emissions (abbreviated as ISOP), red shows Default_ModelE without isoprene drought stress, orange shows DroughtStress_MEGAN3_Jiang, and green shows DroughtStress_ModelE with units of $\text{mg/m}^2/\text{hr}$ of isoprene. (a) Shaded in the grey region from JUL 17 through AUG 31 of 2011, is the period where water stress falls below 0.4 for short periods. (b) Shaded in grey is the MAXVOC period, and shaded in brown is the period of severe/extreme drought from July 17 through August 2012, and shaded in purple is the drought recovery period.

2.6 Offline Isoprene Emissions Model



An offline model was created based on the isoprene emissions formula Eq. (4) of the MEGAN module contained in ModelE in order to develop the new parametrization in a timely fashion without waiting for online transient simulations to complete. ModelE was first run in a default transient simulation with MEGAN2.1 where no isoprene drought stress was applied, referred to as **Default_ModelE**, from which the MEGAN activity factors and variables required to drive the offline calculation of isoprene emissions were output and archived. The offline model was then driven by these outputs at the half hourly timestep to match with the 30-minute timestep in the online calculation of physics and the MEGAN module. The offline model was verified by making sure outputs of isoprene emissions matched the online Default_ModelE simulation. With the verified offline model, different parameterizations of isoprene drought stress could be tested and cross verified with observations at MOFLUX. The offline model is used to derive a model specific α and β threshold (Eq. (6a-6c)) for ModelE in order to create the appropriate parameterization of a model specific isoprene drought stress in ModelE known as **DroughtStress_ModelE**, described in Section 3.3. Since models calculate water stress and $V_{c,max}$ in different ways, the offline model is the necessary step to derive model-specific water stress thresholds to target drought periods and ensure α and β are being applied correctly.

2.7 ModelE Sensitivity Simulations

Four transient global ModelE simulations were configured for the period of 2003-2013 with a three-year spin-up, as described in **Table 1**. A default simulation (Default_ModelE) that set $y_d = 1$ was performed where no isoprene drought stress parameterization was applied. A second simulation named DroughtStress_MEGAN3_Jiang was performed as a sensitivity test to determine the efficacy of the DroughtStress_MEGAN3_Jiang algorithm Eq. (6a-6c), which is not tuned specifically for ModelE, and was originally developed by Jiang *et al.* (2018) as a non-model specific tuned isoprene drought stress formula to be used widely in models. A third simulation was performed with the offline derived ModelE tuned isoprene drought stress parameterization to best fit MOFLUX observations (MOFLUX_DroughtStress) using Eq. (8a-8c) to be described in Section 3.2. A fourth simulation called DroughtStress_ModelE was performed using a subset of parameters derived from MOFLUX_DroughtStress but a different drought activation method in Section 3.3 using Eq. (10a-10b).



Table 1. ModelE Online Transient Simulation Descriptions

Simulation Name	Drought Stress	Isoprene Emission Eqn.	β Threshold	α
1) Default_ModelE	NO	Eq. (4)	N/A	N/A
2) DroughtStress_MEGAN3_Jiang	YES Eq. (6a-6c)	Eq. (7)	$\beta < 0.6$	37
3) MOFLUX_DroughtStress	YES Eq. (8a-8c)	Eq. (9)	$0.25 < \beta < 0.40$	100
4) DroughtStress_ModelE	YES Eq. (10a-10b)	Eq. (9)	$\beta < 4^{\text{th}}$ percentile	100

3. Development of Model specific Drought Stress Parameterization

3.1. MOFLUX Single Site Observational Comparison to Model

Shown in Fig. 1a is the 2011 timeseries of biogenic isoprene flux at the MOFLUX site of two online simulations Default_ModelE (red) and DroughtStress_MEGAN3_Jiang (orange) compared to observations (black). In 2011, Default_ModelE tended to underestimate isoprene flux during onset of drought (July 14 - August 10) and had minor periods of overestimation during drought progression (August 18 – September 2) which was also seen by MEGAN2.1 simulations of Potosnak *et al.* (2014). DroughtStress_MEGAN3_Jiang simulation applied isoprene drought stress from mid-July through September when β fell below the 0.6 threshold identified by Jiang *et al.* (2018). In the DroughtStress_MEGAN3_Jiang simulation it is shown that during the drought progression stage, DroughtStress_MEGAN3_Jiang isoprene is reduced compared to Default_ModelE, but reductions are not strong enough to align with lower observed values for a majority of this period. The timeseries shows that there is little deviation between the Default_ModelE and DroughtStress_MEGAN3_Jiang during the 2011 mild drought.

Shown in Fig. 1b is the 2012 timeseries of biogenic isoprene flux at the MOFLUX site of two online simulations Default_ModelE and DroughtStress_MEGAN3_Jiang compared to observations, with β (blue). Default_ModelE typically underestimates isoprene flux during the MAXVOC period, overestimates during the severe drought period, and reproduces the drought recovery period sufficiently except for September 6 where the model greatly overestimates leading to a peak not matched by observations. During the severe drought period the Default_ModelE mean bias (MB) $\cong 2.20 \text{ mg/m}^2/\text{hr}$ and the normalized mean bias (NMB) $\cong 76.10\%$. β daily average values fell below the 0.60 threshold on June 20 and continued below the threshold through September 3. With the β falling below 0.60, the DroughtStress_MEGAN3_Jiang simulation starts reducing isoprene during the MAXVOC period and continues to reduce through the drought recovery period. This leads to compounding the underestimation during the MAXVOC period, small corrections to overestimation during severe drought but missing the peak overestimations, and too large of reductions of isoprene during drought recovery period. During the severe drought period the MB of



DroughtStress_MEGAN3_Jiang was $\cong 1.61 \text{ mg/m}^2/\text{hr}$ and the NMB was $\cong 55.81\%$. DroughtStress_MEGAN3_Jiang thus decreased the overestimation by $\sim 20.29\%$ during the severe drought period. The timeseries comparison for 2012 indicates the parameters in the Jiang et al. parameterization resulted in only minor improvements in ModelE for the severe drought period, because they were tuned for CLM4.5. The DroughtStress_MEGAN3_Jiang simulation shows that the α and β need to be tuned on a model-by-model basis. Based on these minor improvements, and the differences in how $V_{c,max}$ and β are calculated in CLM4.5 versus Ent TBM, it was clear a model tuned parameterization could be used to further improve the relationship of simulated isoprene emissions during drought.

3.2 Site Tuned MOFLUX_DroughtStress Parameterization

Using the offline isoprene emissions model (Section 2.6) driven by catalogued variables from each time step of the **Default_ModelE** simulation and the MOFLUX biogenic isoprene flux measurements for 2012, we describe here how a water stress threshold to target severe/extreme drought periods and a model appropriate empirical variable (α) were derived to create the isoprene drought stress parameterization based upon the framework of Eq. (6a-6c), called **MOFLUX_DroughtStress**. MOFLUX_DroughtStress was developed to target the 2012 severe drought period shown in Fig. 1b as this period is when the model overestimates despite observations showing decreasing emissions during drought. The water stress threshold range targeting the severe drought period determines when the isoprene drought stress is applied and it is bounded to exclude the period of drought recovery and the onset of drought when isoprene emissions are still increasing. The range of β specific to ModelE is 0.25 to 0.40 during the severe drought period, which differs from the CLM4.5 threshold of 0.60 as it is a model specific parameterization. Isoprene drought stress in MOFLUX_DroughtStress is thus applied only when $\beta < 0.40$, and at all other β values $y_d = 1$.

To find the empirical variable, α , an offline sensitivity analysis was conducted using the offline isoprene emissions model with 0.25 to 0.40 as the β threshold to activate isoprene drought stress. The PFT weighted value of $V_{c,max}$ and β were used to calculate the y_d in the offline isoprene emissions model. A range of α values from 60 to 160 were tested in Eq. (8a-8c) to find y_d . y_d dependence on the value of α was fed into Eq. (9) to output offline isoprene emissions. The offline modeled emissions from Eq. (9) were evaluated against observed isoprene fluxes at MOFLUX, and it was determined that $\alpha = 100$ gave the best fit and strongest relationship between the offline modeled emissions and measured isoprene at MOFLUX. The α variable, though empirically derived, is strongly related to the model specific $V_{c,max}$ which is why our alpha differs from DroughtStress_MEGAN3_Jiang, where $\alpha = 37$. Based on the offline emissions comparisons to observed it was determined that **MOFLUX_DroughtStress** is defined as follows:

$$y_d = 1 \quad (\beta \geq 0.4) \quad (8a)$$



$$y_d = \frac{(v_{c,max} \times \beta)}{\alpha} (0.25 < \beta < 0.40) \text{ where } \alpha=100 \quad (8b)$$

$$y_d = 1 (\beta \leq 0.25) \quad (8c)$$

$$Isoprene_i = (1 \times 10^{-9} / 3600) \times (EF_{i,isoprene} \times PFTboxf_i) \times y_{LAI} \times y_A \times y_d \times y_{CO_2} \times (y_P \times y_{TLD}) \times SF_{isoprene} \quad (9)$$

Where y_d uses the area weighted average over PFTs of $v_{c,max}$ and β in Eq. (8a-c), and thus y_d in Eq. (9) is not a function of PFT, which differs from DroughtStress_MEGAN3_Jiang Eq. (7) where y_d is a function of PFT.

MOFLUX_DroughtStress simulation with isoprene drought stress applied Eq. (8a-8c) is found to reduce the MB at the MOFLUX site to ≈ 0.04 mg/m²/hr during the 2012 severe drought period, indicating the parameterization is able to correct the model overestimation of isoprene emissions. The NMB decreased to $\approx 1.53\%$, indicating a $\sim 74.57\%$ reduction compared to Default_ModelE. Large improvements were not expected for 2011 as this algorithm was designed to target severe/extreme drought. Despite the better agreement between measured and modeled fluxes in MOFLUX_DroughtStress at the MOFLUX site, the regional analysis described below determined that water stress values are region specific and a new approach was needed in order to make the algorithm applicable for other regions in the global model.

3.3 New Percentile Threshold Isoprene Drought Stress Parameterization

After implementing MOFLUX_DroughtStress in ModelE, we found for JUN-AUG 2011 isoprene emissions reductions for the southeastern (SE) U.S. defined as (96-75°W, 25-38°N) of approximately -3.5%, -7.2%, -5.7% respectively. These regional reductions were smaller than expected as the SEUS 2011 was a spatially extensive severe drought over a largely forested and vegetated region. The US Drought Monitor (USDM) reported that the southeast area in moderate to exceptional drought for JUN-AUG 2011 was 63%, 61%, and 55% respectively. Other studies for other regions of the world have reported during severe drought that reductions in isoprene vary by region and have a large uncertainty. For example, Huang et al. (2015) reported using different soil moisture products isoprene reductions of 12-70% for Texas. Others showed reductions up to a maximum of 17% (Jiang et al. 2018; Wang et al. 2021). The reason why MOFLUX_DroughtStress falls on the lowest end of reported isoprene reductions for the regional analysis is probably because drought stress activation was calibrated to water stress ranges at a single site. As water stress is expected to vary regionally, a new regional method was needed in order to simulate drought stress effects globally.

A new parameterization was designed to not only work at MOFLUX since this is the site used for validation, but capture isoprene drought signals for other regions. To do so, we first simulated daily averaged water stress during the growing season for ten years (2003-2012) at MOFLUX, a total of 2450 days. It was determined that water stress was less than the 0.4



threshold for 102 days, a percentage of $\sim 4.16\%$. For simplicity, we rounded the percentage to 4%. The new approach then relied upon finding the 4th percentile water stress value across ten years of daily water stress per grid and for each individual month in order to build a parameterization that would capture regional and seasonal variability in water stress in ModelE. This new drought stress parameterization is known as DroughtStress_ModelE and uses the same alpha ($\alpha=100$) as MOFLUX_DroughtStress and is applied as weighted average per PFT. What makes this different from the previous approach, MOFLUX_DroughtStress, is that the water stress threshold used to apply drought stress is based on the model's unique lowest 4th percentile of water stress on a grid-by-grid basis and is not based on the absolute values of water stress at a single site (i.e., MOFLUX). The 4th percentile of daily water stress was used as the trigger for drought stress activation. The parameterization for **DroughtStress_ModelE** is Eq. (10a-10b):

$$y_d = 1 \quad \text{when } (\beta \geq 4^{\text{th}} \text{ percentile}) \quad (10a)$$

$$y_d = \frac{(v_{c,max} \times \beta)}{\alpha} \quad \text{when } (\beta < 4^{\text{th}} \text{ percentile}), \text{ where } \alpha=100 \quad (10b)$$

A global transient simulation was run from (2003-2013) applying Eq. (10a-10b) globally, called DroughtStress_ModelE in order to determine the effects of the isoprene drought stress parameterization and to see if it captures the signal of the 2011 SE drought. DroughtStress_ModelE for JJA 2011 showed isoprene emissions percent reductions for the SE of approximately -9.6%, -5.9%, and -12.7% respectively. These reported reductions are a factor of two greater than MOFLUX_DroughtStress for the same period, and are in the mid-range of reported isoprene reductions during drought. A complete timeseries of isoprene emissions at MOFLUX for all four simulations as described by **Table 1** is shown in SI Fig. S2a-b for 2011 and 2012.

620

621 **3.4 DroughtStress_ModelE Evaluation at MOFLUX**

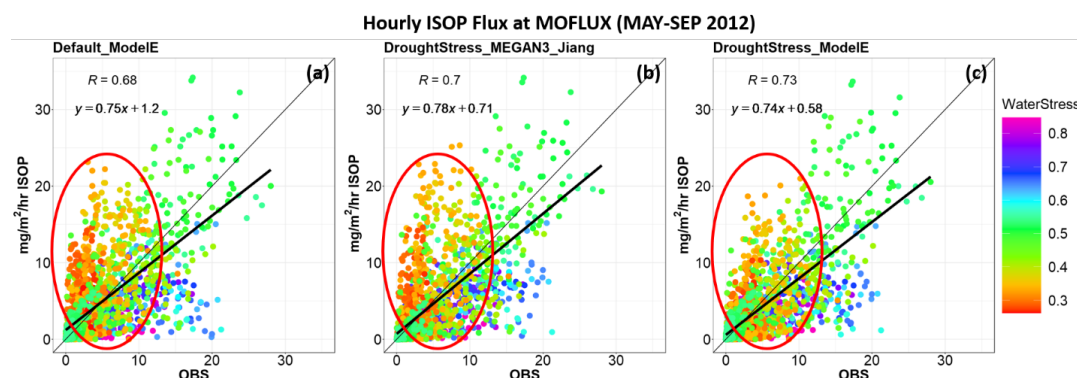
During 2011 at the MOFLUX site, there were only small differences between Default_ModelE and DroughtStress_ModelE. The scatterplots of isoprene emissions at the MOFLUX site for the summer of 2011 show the hourly correlation coefficient between modeled and observed isoprene fluxes showed minor improvement from 0.77 to 0.78, with minor changes in slope and y-intercept (SI Fig. S3a,c). The diurnal cycles for 2011 included in (SI Fig. S4a) showed that neither MOFLUX_DroughtStress nor DroughtStress_ModelE altered the diurnal cycle in comparison to Default_ModelE. For 2011, all four simulations underestimate the diurnal cycle for MAY-AUG. Large improvements due to the applications of the Eq. (10a-10b) were not expected for 2011 as this algorithm was designed to target severe/extreme drought and not less severe drought conditions.

632

During the severe drought period of 2012 at MOFLUX, the β values fell below the 4th percentile thresholds for July-August, and isoprene drought stress was applied leading to reductions in the overestimation shown by Default_ModelE. DroughtStress_ModelE had a MB



636 $\cong 0.42 \text{ mg/m}^2/\text{hr}$ and a NMB $\cong 14.5\%$. DroughtStress_ModelE reduced overestimation by $\sim 61.6\%$
 637 compared to Default_ModelE, which is a similar statistical improvement compared to
 638 MOFLUX_DroughtStress during the severe drought period as the parameterizations were
 639 designed in a similar manner. The scatterplots of isoprene emissions at the MOFLUX site for the
 640 summer of 2012 show the hourly correlation coefficient between observations and simulations
 641 increased from 0.68 in Default_ModelE to 0.73 in DroughtStress_ModelE (Fig. 2a,c). In Fig. 2
 642 changes are clearly seen in the cluster of β values lower than 0.4 (shown by red oval) indicating
 643 a reduction in overestimation during severe drought.
 644



645 Figure 2. Scatterplots (a-c) show hourly simulated isoprene emissions compared to observed for MAY-SEP 2012 at the
 646 MOFLUX site and the units are $\text{mg/m}^2/\text{hr}$ of isoprene. Column 1-3 indicate simulations Default_ModelE,
 647 DroughtStress_MEGAN3_Jiang, and DroughtStress_ModelE respectively. The hourly averaged points are color coded by
 648 water stress.

649
 650 DroughtStress_ModelE with decreases in y-intercept, increasing correlation coefficient, and
 651 minor change in slope compared to Default_ModelE suggests it has better performance in
 652 simulating isoprene emissions during severe and extreme drought at MOFLUX during the
 653 summer of 2012. The daily correlation coefficient increased from 0.64 to 0.73 during severe
 654 drought in DroughtStress_ModelE (SI Fig. S5a,c). In addition, DroughtStress_ModelE
 655 reproduces the diurnal cycle of isoprene emission from MAY-SEP 2012 shown in (SI Fig. S4b)
 656 and corrects the overestimation of the Default_ModelE during the peak hours 10-15 LST.
 657 Overall, there is model agreement between measured and modeled fluxes in
 658 DroughtStress_ModelE indicating it is a suitable model-tuned parameterization for estimating
 659 isoprene emissions during severe drought at the MOFLUX site.

661 4. Model response to drought parameterization: Global/Regional Evaluation of 662 DroughtStress_ModelE

663 The impact of applying isoprene drought stress in DroughtStress_ModelE globally on the
 664 annual emissions of isoprene from 2003-2013 is shown in Table 2. The yearly global reduction



of isoprene emissions ranges from $\sim -0.9\%$ to -4.3% . The global decadal average from 2003-2013 is $\sim 533 \text{ Tg yr}^{-1}$ of isoprene in Default_ModelE and $\sim 518 \text{ Tg yr}^{-1}$ of isoprene in DroughtStress_ModelE, a reduction of 2.7%, which is equivalent to $\sim 14.6 \text{ Tg yr}^{-1}$ of isoprene. On a global scale these changes average under 3%, but for high isoprene emission regions such as the Southeast U.S. during drought periods there are larger impacts as shown below.

Table 2. Global Annual Tg of Isoprene (2003-2013)

Global Annual Isoprene Emissions (Tg)				
Year	Default_ModelE	DroughtStress_ModelE	Diff (Tg Isoprene)	% Diff
2003	557.5	533.4	24.1	-4.3
2004	557.6	535.4	22.2	-4.0
2005	578.6	562.1	16.5	-2.9
2006	537.5	522.9	14.6	-2.7
2007	527.2	515.8	11.4	-2.2
2008	499.2	494.9	4.3	-0.9
2009	522.3	508.4	13.9	-2.7
2010	542.5	526	16.5	-3.0
2011	508.3	498.8	9.5	-1.9
2012	516.1	503.4	12.7	-2.5
2013	512.5	497.5	15	-2.9

Figure 3 shows the global nine-year average of isoprene emissions and tropospheric HCHO column densities (ΩHCHO) of the lowest twenty layers of the model during JJA from 2005-2013. Due to extremely limited in situ measurements of isoprene emissions during drought, satellite-retrieved ΩHCHO , the high yield oxidation product of isoprene, can be used as a proxy for isoprene emissions on the monthly scale (Zhu *et al.* 2016). Here we used ΩHCHO from OMI (Ozone Monitoring Instrument) on the Aura satellite starting in 2005. Level 3 total column weighted mean was regridded from its original resolution of $0.1^\circ \times 0.1^\circ$ to match ModelE's horizontal resolution of $2^\circ \times 2.5^\circ$, and the daily data was aggregated to monthly mean (https://cmr.earthdata.nasa.gov/search/concepts/C1626121562-GES_DISC.html) (Chance 2019). OMI satellite data was filtered with the data_quality_flag, cloud fractions less than 0.3, solar zenith angles less than 60, and values within the range of -0.5 to $10 \times 10^{16} \text{ molecules cm}^{-2}$ were used (Zhu *et al.* 2016). A factor of 1.59 is applied to the OMI vertical column density (VCD) to correct the mean bias (Kaiser *et al.* 2018). Figures 3c,3f show the percent difference of isoprene emissions and ΩHCHO and shown in blue are the decreases in DroughtStress_ModelE globally. Figures 3d-e is OMI ΩHCHO and Default_ModelE simulated ΩHCHO . It is important to note the difference in scales as Default_ModelE is overestimating ΩHCHO in regions such as the SE U.S. for every June-July from the 2005-2013 period with a regional mean scale factor of ~ 0.56 and ~ 0.80 when the SE boundary is extended westward to include portions of Texas. These overestimates in the SE U.S. are also reported by (Kaiser *et al.* 2018) where they saw a 50%



overestimate by GEOS-Chem with MEGAN2.1 simulations compared to SEAC⁴RS observations. While applying isoprene drought stress leads to reductions in Ω HCHO as shown by Fig. 3f, this reduction is limited to drought-stricken regions and periods and not designed to correct for the systematic biases of HCHO in ModelE. The overestimation of Ω HCHO in Default_ModelE will require further study and could be due to several reasons such as emissions error, incorrect spatial gradient of OH, oxidation, or incorrect application of the sink of glyoxal (Volkamer *et al.* 2007; Wells *et al.* 2020). This version of ModelE also lacks direct emissions of HCHO from anthropogenic sources, which may result in the lower vertical deposition, and, due to the short lifetime, the higher than observed HCHO column over portions of the U.S., and lower in other regions.

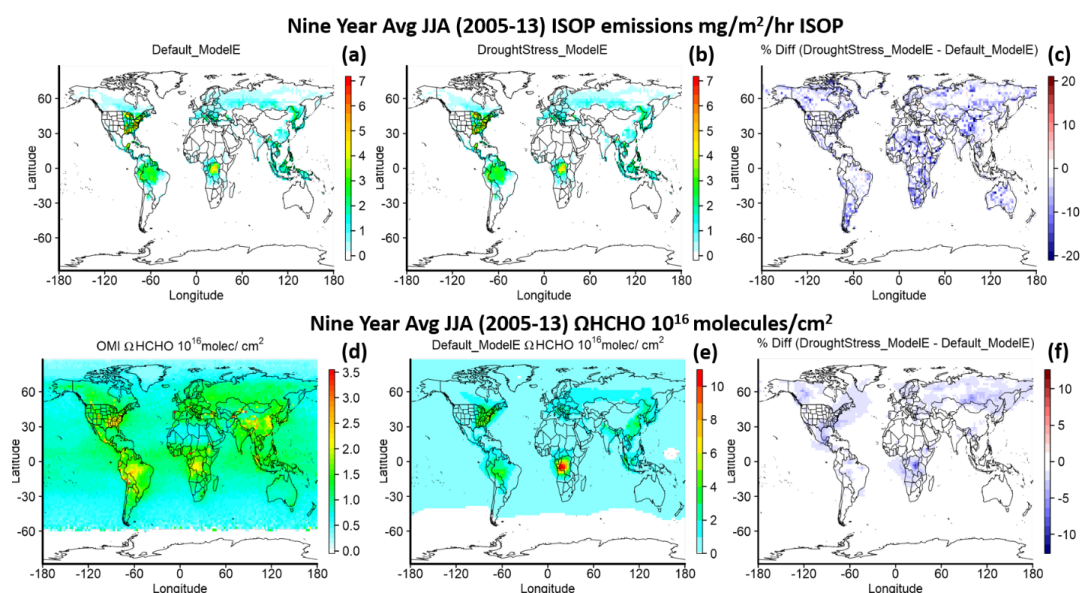


Figure 3. Global nine-year average of JJA from 2005-2013 of isoprene emissions (first row) for Default_ModelE (a), DroughtStress_ModelE (b) and percent difference between DroughtStress_ModelE and Default_ModelE (c), and Ω HCHO (second row) for OMI (d), Default_ModelE (e) and percent difference between DroughtStress_ModelE and Default_ModelE (f). Note the different color scales between (d) and (e).

Four global isoprene emission hotspots are selected to showcase the changes in isoprene emissions. The geographic regions are defined as East U.S. (Eastern U.S.: 65-105°W, 25-50°N), SA (Amazon: 40-80°W, 30°S-7°N), AF (Central Africa: 10-40°E, 15°S-10°N), and SE Asia (Southeast Asia: 100-150°E, 11°S-38°N) as shown in (SI Fig. S6). Figure 4 shows the relationship of dryness categorized by SPEI (Standardized Precipitation-Evapotranspiration Index) and relative difference in isoprene emissions between DroughtStress_ModelE and Default_ModelE from 2005-2013 for the growing season in the northern hemisphere and spring/summer in the southern hemisphere for the four global isoprene hotspots. SPEI is a



716 multiscalar climatic index that represents duration of drought in a region and is based on a
717 climatic water balance approach which considers the impact of temperature and
718 evapotranspiration (Beguería *et al.* 2010; Vicente-Serrano *et al.* 2010; Beguería *et al.* 2014). To
719 identify the extent of drought impacts and differentiate from normal variability in the
720 hydrological cycle, one-month SPEI is used to identify drought periods of duration extending
721 beyond a single month. Default_ModelE simulation variables were used to calculate modeled
722 SPEI at the resolution of $2^{\circ} \times 2.5^{\circ}$. Positive SPEI typically indicates wet conditions and dry
723 conditions are indicated by negative values. Drought conditions are indicated by $\text{SPEI} \leq -1.3$,
724 normal conditions $-0.5 \leq \text{SPEI} \leq 0.5$, and wet conditions $\text{SPEI} \geq 1.3$ following the (Wang *et al.*
725 2017) approach. For the four regions the average percent difference in isoprene emissions for
726 March-October for northern hemisphere regions and September-February for southern
727 hemisphere regions from 2005-2013 is $\sim -2.62\%$ for the East U.S., the Amazon (SA) $\sim -3.01\%$,
728 Central Africa (AF) $\sim -2.64\%$, and Southeast Asia (SE Asia) $\sim -3.10\%$. The scatterplots for the
729 four hotspots show decreasing isoprene emissions across all dryness conditions. The decreases in
730 isoprene emissions for the four regions are not seen exclusively when SPEI indicates dry
731 conditions, which indicates simulated water stress as shown by model does not align exactly with
732 SPEI drought indicated conditions.

733



2005 - 2013 SPEI vs ISOP Delta (DroughtStress_ModelE-Default_ModelE)

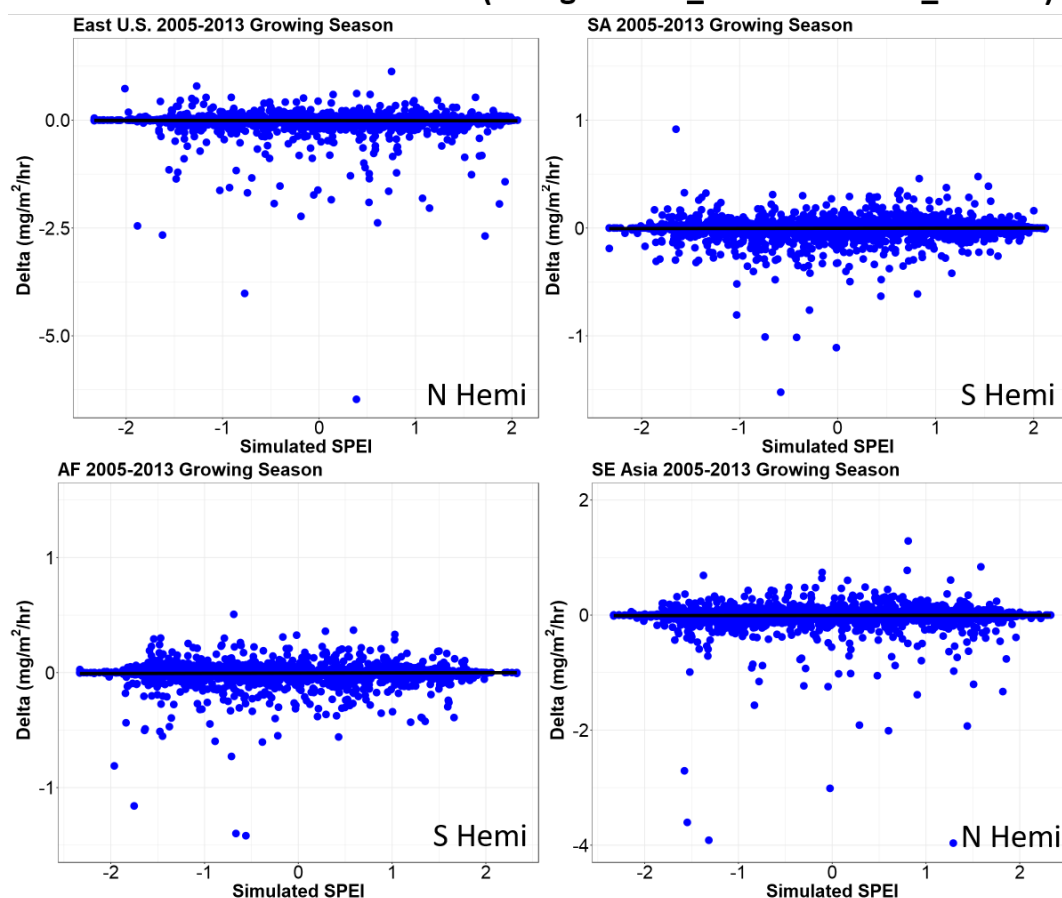


Figure 4. The scatterplots of four global isoprene hotspot and their relative differences in isoprene emissions ($\text{mg/m}^2/\text{hr}$ isoprene) in relationship to simulated SPEI from 2005-2013 during the growing season is shown. The four regions of focus are Eastern U.S. (East), Amazon (SA), Central Africa (AF), and Southeast Asia (SE Asia). The regions of East and SE Asia are in the northern hemisphere and the growing seasons is from (March-October). The hotspots of SA and AF are in the southern hemisphere and the growing season is during spring/summer (September-February).

Narrowing the focus from global to the U.S., to illustrate the long-term difference between DroughtStress_ModelE and Default_ModelE, a timeseries from 2005-2013 is shown in Fig. 5 of the continental U.S. for two regions West ($105\text{-}125^\circ\text{W}$, $25\text{-}50^\circ\text{N}$) and East ($65\text{-}105^\circ\text{W}$, $25\text{-}50^\circ\text{N}$) indicating the percent difference in ΩHCHO and isoprene emissions corresponding to percent area that is dry ($\text{SPEI} < -0.5$). The map showing the regions West and East is located in (SI Fig. S7). The western U.S. (West) despite having a much smaller magnitude of isoprene emissions does see reductions in isoprene which is mimicked on a lesser scale by reductions in ΩHCHO . For the Eastern U.S. (East) there are clear decreases in isoprene emissions and ΩHCHO during



748 the droughts of 2007, 2011, and 2012. Focusing on the East timeseries, the maximum percent
749 difference between simulations DroughtStress_ModelE and Default_ModelE for isoprene
750 occurred from AUG-OCT 2007 approximately -4.5%, -7.4%, and -4.6% with corresponding
751 decreases in ΩHCHO of $\sim -4.1\%$, -5.4% , and -3.6% respectively. For 2011 the maximum percent
752 difference in isoprene emissions occurred SEP-NOV and was $\sim -9.0\%$, -8.7% , -8.3% and the
753 percent difference in ΩHCHO was $\sim -5.9\%$, -3.6% , and -2.6% . For 2012 the maximum percent
754 difference occurred from AUG-OCT and the difference in isoprene was $\sim -5.1\%$, -8.8% , and -
755 10.8% and the difference in ΩHCHO was $\sim -2.8\%$, -4.0% , and -2.7% .
756

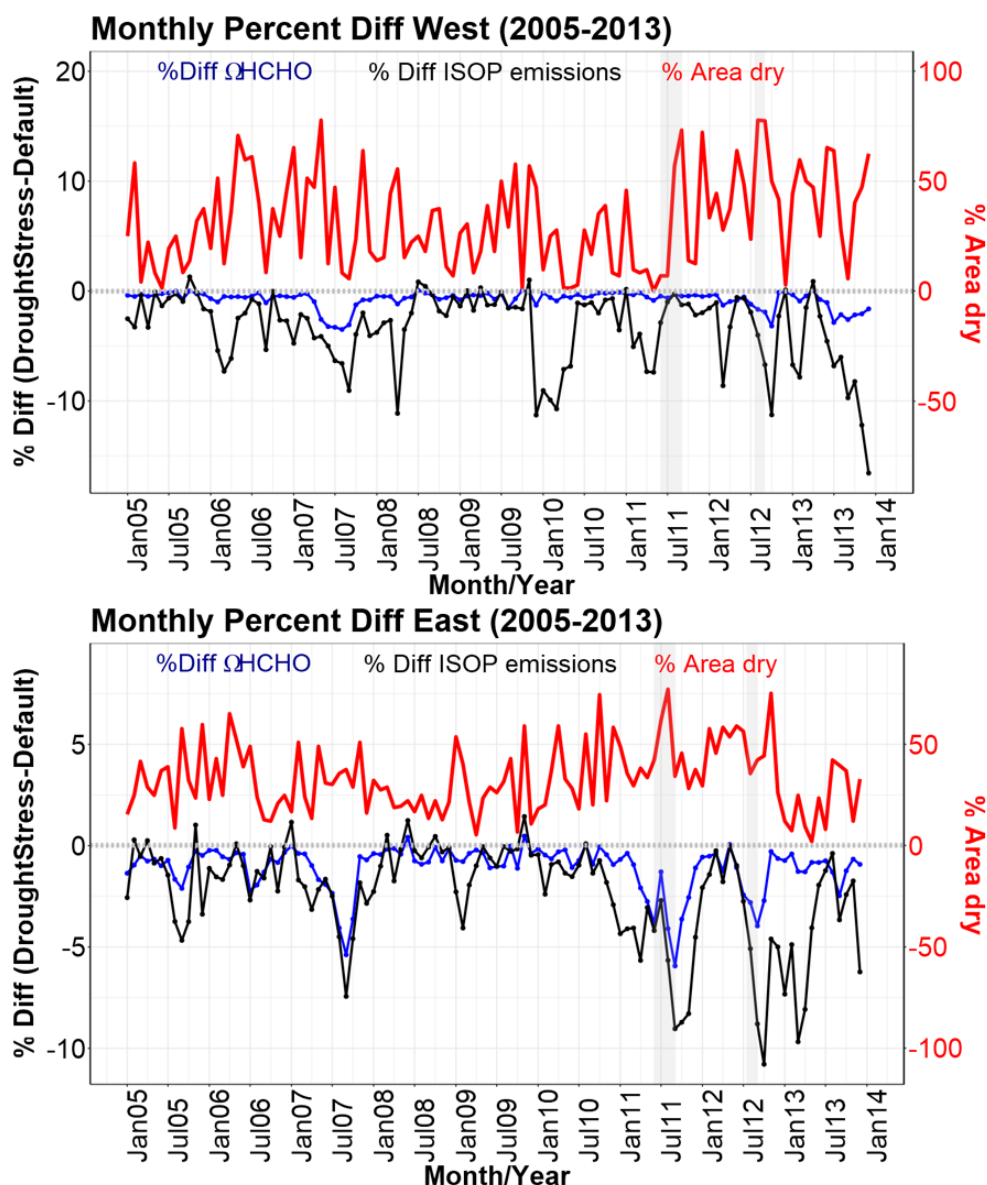


Figure 5. The percent difference of ΩHCHO and isoprene emissions from 2005-2013 in relationship to percent area dry for two regions of the U.S. West (top figure) and East (bottom figure) is shown. Percent area dry is indicated by SPEI < -0.5. The first grey shaded rectangle indicates the time period of the 2011 drought at MOFLUX from June to August 2011. The second grey shaded rectangle indicates the 2012 severe drought at MOFLUX from July 17 through August. These time periods are added to the timeseries to highlight when they occurred.

762

Figure 6 displays spatial maps of ΩHCHO during the summer (JJA) of three drought years 2007, 2011, and 2012. The summers of 2007 and 2011 were drought periods in the U.S. with

764



2007 being a less severe drought than 2011 in the SE U.S. The drought of 2012 was focused more on the Great Plains (GP) region. The spatial maps show the reduction in ΩHCHO in panels 6c, 6f, and 6i due to the inclusion of isoprene drought stress. Based on the spatial differences in ΩHCHO , three regions of the greatest reduction in percent difference in ΩHCHO column are selected for the three drought years of 2007, 2011, and 2012, respectively. The three geographic regions are shown in Fig. 7 and defined as SE1 (Southeast Region1: 75-93°W, 31-39°N), SE2 (Southeast Region2: 75-101°W, 29-37°N), and GP (Great Plains: 89-100°W, 33-43°N). During JJA for 2007 the SE1 region has an average percent difference in ΩHCHO of -6.46%, during JJA 2011 the SE2 region has a percent difference of -7.58%, and the GP region during JJA 2012 has average percent difference of -3.29%.

775

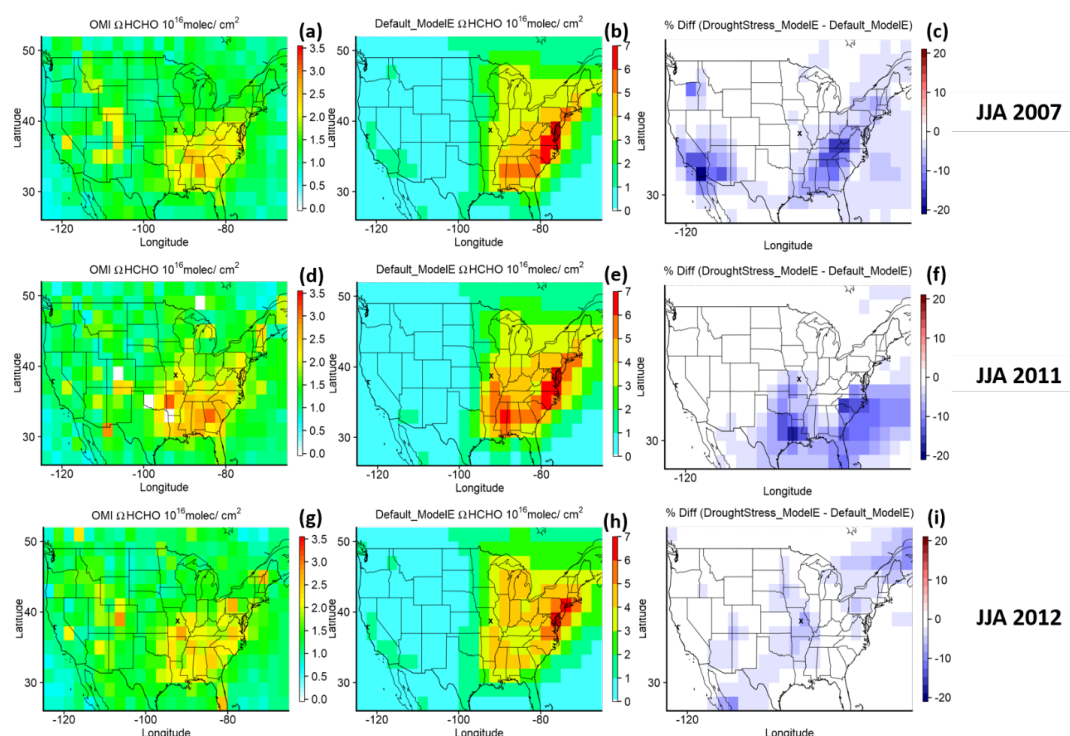


Figure 6. The ΩHCHO column in units of molecules/cm² for OMI, Default_ModelE, and the percent difference between DroughtStress_ModelE and Default_ModelE across the U.S. during the summer of drought years 2007, 2011, and 2012 is shown. X indicates the location of the MOFLUX site on the spatial maps.

779

Figure 7 shows the timeseries for the three regions of SE1 during 2007, SE2 for 2011, and GP for 2012 drought. In the SE1 region during the period of maximum isoprene difference from AUG-OCT 2007 shaded in grey on the timeseries, DroughtStress_ModelE reduced NMB of ΩHCHO by ~19.3%. The isoprene percent difference for this period was approximately -9.0%, -17.5%, and -13.2%. The ΩHCHO percent difference for the SE1 region from AUG-OCT 2007



785 was approximately -8.4%, -12.1%, and -7.3%. In the SE2 region the maximum isoprene
 786 difference period for AUG-NOV 2011, DroughtStress_ModelE decreased Ω HCHO NMB by
 787 $\sim 15.3\%$. The monthly isoprene percent difference for SE2 during this period was approximately
 788 -16.1%, -18.6%, -14.7%, and -13.9% while the Ω HCHO percent difference was $\sim -10.0\%$, -
 789 11.2%, -6.6%, and -4.6% respectively. In the GP region during SEP-NOV 2012, the isoprene
 790 percent difference for GP during SEP-NOV 2012 was approximately -5.4%, -14.2%, and -11.1%
 791 and the Ω HCHO percent difference was $\sim -2.8\%$, -2.4%, and -0.4% respectively. The small
 792 change in HCHO column despite estimated larger changes in isoprene emissions is probably due
 793 to the suppression of oxidants such as hydroxyl radicals (OH) by isoprene under low-NO_x
 794 conditions in the GP region (Wells *et al.* 2020).

795
 796 It is well established that biogenic isoprene, the most abundant BVOC, is a highly reactive
 797 species. In the presence of nitrogen oxides (NO_x), BVOCs contribute to the formation of
 798 tropospheric O₃. Oxidation of BVOCs also produces secondary organic aerosols, a major
 799 component of fine particulate matter (PM_{2.5}). PM_{2.5} and O₃ have been previously linked to
 800 change during drought with adverse effects on air quality (Wang *et al.* 2017). It is thus important
 801 to show the impact of drought-induced changes in isoprene emissions on O₃ and PM_{2.5}. The
 802 scatterplots in Fig. 7 show the relationship between observed and simulated O₃ during the
 803 drought period of maximum percent difference highlighted on the timeseries for the
 804 corresponding region. PM_{2.5} comparison to observed is not shown here due to Default_ModelE
 805 underestimating PM_{2.5} across all three regions SE1, SE2, and GP, and thus no improvements
 806 were seen due to the inclusions of DroughtStress_ModelE. The observational O₃ data is a
 807 combination of hourly data from the EPA-AQS (U.S. Environmental Protection Agency (EPA)
 808 Air Quality System), CASTNET (Clean Air Status and Trends Network), and NAPS (National
 809 Air Pollution Surveillance) networks. The observational O₃ datasets was gridded and interpolated
 810 for comparison to a gridded model (Schnell *et al.* 2014). The hourly gridded observations were
 811 then averaged onto a monthly scale for comparison with model results. Shown in Fig. 7 the SE1
 812 region saw improvement in O₃ from AUG-OCT 2007, where the correlation coefficient (R)
 813 increased from 0.51 in Default_ModelE to 0.60 in DroughtStress_ModelE and the slope of the
 814 linear regression also improved significantly. The SE2 region from AUG-NOV 2011 saw a slight
 815 improvement in the slope of the linear regression but no change in R. The GP region from SEP-
 816 NOV 2012 saw a slight improvement in R but no change in the correlation slope between
 817 Default_ModelE and DroughtStress_ModelE. During non-drought periods of 2008, 2010, and
 818 2013 compared to their respective drought periods of 2007, 2011, and 2012 there was no large
 819 changes in O₃ or Ω HCHO statistics as expected since isoprene drought stress is only supposed to
 820 effect drought periods. During the drought periods of 2007, 2011, and 2012 the model predicts
 821 higher mean O₃ and Ω HCHO than the non-drought years. The analysis of these drought years
 822 and periods of the greatest percent difference leads to the conclusion of isoprene drought stress
 823 improves Ω HCHO simulation and O₃ simulation during drought periods.



824

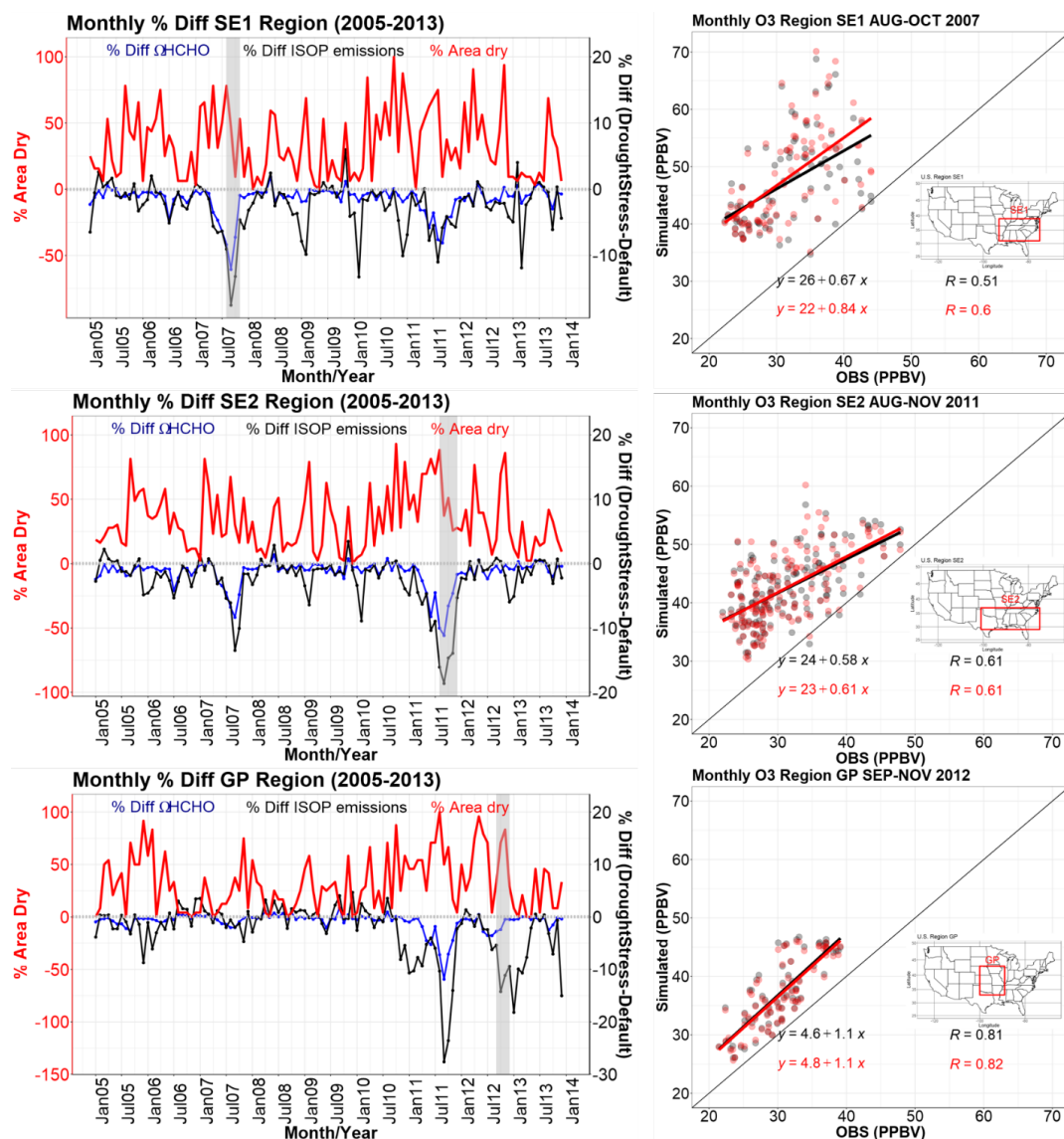


Figure 7. The timeseries from 2005-2013 of percent area dry on y-axis shown in red and percent difference in ΩHCHO (blue) and isoprene emissions (black) between DroughtStress_ModelE and Default_ModelE for the 3 regions SE1, SE2, and GP on the second y-axis is shown. Shaded in grey are the time periods of maximum percent difference of isoprene emissions during the drought years. The scatterplots show the relationship between observed O_3 (ppbv) and simulated O_3 during the shaded grey time periods on the timeseries for Default_ModelE in black and DroughtStress_ModelE in red for the SE1 during 2007, SE2 during 2011, and GP during 2012. Maps showing the geographic regions are inset into the scatterplots. The regions spatial extent is based on region of maximum percent difference in Fig. 6c,f,i.

832



5. Discussion and conclusions

Drought is a hydroclimatic extreme that causes perturbations to the terrestrial biosphere. As a stressor for vegetation, drought can induce changes to vegetative emissions known as BVOCs (Biogenic Volatile Organic Compounds). Biogenic isoprene represents about half of total BVOC emissions and is a precursor to ozone (O_3) and secondary organic aerosol (SOA), both of which are climate forcing species. In order to simulate isoprene flux during drought and the feedbacks associated with these complex BVOC-chemistry-climate interactions, we implemented the MEGAN (Model of Emissions of Gases and Aerosols from Nature) isoprene drought stress parameterization, y_d , into NASA GISS (Goddard Institute of Space Studies) ModelE, a leading Earth System Model. Four online transient simulations were performed from 2003-2013, a Default_ModelE without y_d , DroughtStress_MEGAN3_Jiang using the parameterization developed by (Jiang *et al.* 2018), and a model-tuned parameterization developed for ModelE based on the MOFLUX Ameriflux site observations (MOFLUX_DroughtStress). The fourth simulation implemented isoprene drought stress using a grid-by-grid approach to capture regional changes in isoprene during drought known as DroughtStress_ModelE. The model-tuned parameterization (MOFLUX_DroughtStress and DroughtStress_ModelE) was developed using an offline model of emissions to create a model specific empirical variable and water stress threshold, since key variables $V_{c,max}$ (photosynthetic parameter) and water stress (β) are parameterized differently across models. Observational measurements of isoprene flux during the severe drought of 2012 at the MOFLUX site were used for validation of parameterization. It was found that DroughtStress_ModelE corrects the overestimation of emissions during the phase of severe drought at MOFLUX. Previously, this reduction during drought was not included in BVOC emission models due to the lack of a drought stress term. Globally the decadal average from 2003-2013 in Default_ModelE was ~533 Tg of isoprene and ~518 Tg of isoprene in DroughtStress_ModelE. DroughtStress_ModelE was validated using observational satellite $\Omega HCHO$ column from the Ozone Monitoring Instrument (OMI) and using O_3 observations across regions of the U.S. to examine the effect of drought on atmospheric composition. It was found that the inclusion of isoprene drought stress reduced the overestimation of $\Omega HCHO$ in Default_ModelE during the 2007 and 2011 southeastern U.S. droughts and led to improvements in simulated O_3 during drought periods. The inclusions of a grid specific percentile isoprene drought stress is model specific and the reduction of isoprene seen in models will depend on each models mean bias and parameterizations of $V_{c,max}$ and water stress. ModelE's modest signal can be explained by underestimating isoprene emissions during the early stages of drought and by not having a high mean bias during severe drought.

Our analysis of isoprene drought stress leads to the recommendation that each model should arrive at a tuning of their water stress parameters based on the magnitude of water stress occurring during simulated drought and a unique alpha should be derived. Each land surface model (LSM) has a unique hydrology scheme (with different soil layering approaches and soil physics treatments), and any variables that depend on response to soil moisture -- whether



chemical, physical, or biological -- must be tuned due to the fact that soil moisture in LSMs is being averaged over a grid cell whereas in nature soil moisture is heterogeneous at spatial scales down to the plot level. The resulting parameterization, since it relies on model specific variables, would be well suited for future or historical simulations. The current approach also requires vegetation-coupled land surface models that have photosynthesis models that use $V_{c,max}$ and β , and many current general circulation models (GCM) with less process-based vegetation schemes do not have these variables readily available.

Besides tuning responses to drought, the light response of isoprene emissions may not be well captured in a simple factor like the PCEE. Vegetation models differ in their approach to leaf-to-canopy scaling. Some ESMs vegetation models have more sophisticated canopy radiative transfer submodels that capture layering and sunlit/shaded leaf area. Future isoprene modeling investigations could make use of the ability of these canopy models to calculate isoprene emissions with leaf-level responses to the heterogeneous light in canopies. Unger *et al.* (2013) implemented such a leaf-to-canopy scaling of isoprene emissions previously in the Ent TBM through a leaf-level isoprene model as a function of leaf-level gross primary production (GPP). Since the Ent TBM scales stomatal conductance with drought stress, and hence also GPP, this intrinsically results in isoprene emissions responsiveness to drought stress. The main challenge will be to find consensus about the fundamental process-based physics of isoprene emissions at the leaf level. The method of Unger *et al.* (2013) was not used for this paper in order to preserve the MEGAN3 features and test this particular isoprene drought stress parameterization.

A limitation of our tuning method for applying isoprene drought stress is that there does not appear to be a strong relationship between SPEI and water stress, which makes it challenging to determine when the algorithm should be applied during severe drought. This is why the current application is limited and based on the single MOFLUX site where water stress values and the corresponding decreases of isoprene during severe drought were observed. Possible future work of the satellite Cross-track Infrared Sound (CrIS) isoprene measurements (Wells *et al.* 2020) may be used to develop a drought algorithm that is not based on a single site and provide a more dynamic drought stress algorithm for capturing the decrease of emissions during severe drought. The reduction of isoprene in the model also depends on how dry (low values of water stress) the model is. If the model is too dry or if isoprene emissions are already overestimated there will be larger reductions in isoprene than reported here in ModelE, with larger feedbacks on O_3 , SOA, and $\Omega HCHO$ column. Models that are not severely overestimating during severe drought will show modest reductions like ModelE. It is important to note that the application of isoprene drought stress in this paper is designed to reduce emissions during severe drought. Future work could focus more on the parameterization of isoprene emissions during mild or early stages of drought when isoprene emissions might be increasing and as we see in ModelE the model underestimates during this period. Overall, the strength of the reduction signal of isoprene depends on the model, and for models overestimating isoprene the application of isoprene



drought stress into the model could improve model simulations significantly. Recent published work has also brought up the importance of drought duration as an important factor to consider in further isoprene drought stress parameterization (Li *et al.* 2022). Future work on developing drought parameterizations should focus on capturing the increasing signal of isoprene at the start of drought, the reduction signal during severe drought, while also considering a time component because eventually plants can reach a stage of emission cessation.

In summary, this paper demonstrates why isoprene response to drought stress is model specific and should be tuned on a model-by-model basis, and details a new method for implementing isoprene drought stress to reduce isoprene emissions during severe drought in ModelE. This new method uses a grid-by-grid percentile threshold based on simulated water stress and can be used by many models to show regional changes in isoprene emissions during severe drought and their associated feedbacks on Ω HCHO and O_3 . With more severe droughts predicted in the United States for the 21st century (Dai 2013), this is a first look into model performance for analyzing how BVOC emissions change during drought conditions using GISS ModelE for regions in the U.S.

6. Acknowledgements

E.K., Y.W. and A.G. would like to acknowledge the support and funding from the NASA ACMAP Program (80NSSC19K0986). E.K. and Y.W. would also like to acknowledge the support and funding of NASA Fellowship Grant (80NSSC18K1704) and thank support of NASA technical advisors at Goddard Institute of Space Studies. Resources supporting this work were provided by the NASA High-End Computing (HEC) Program through the NASA Center for Climate Simulation (NCCS) at the Goddard Space Flight Center. GISS authors acknowledge funding from the NASA Modeling and Analysis program.

7. Data availability

ModelE is publicly available at <https://simplex.giss.nasa.gov/snapshots/> and O_3 and $PM_{2.5}$ observational data available for download via https://aq5.epa.gov/aq5web/documents/data_mart_welcome.html. Observational isoprene measurements at MOFLUX are from Potosnak *et al.* 2014 and Seco *et al.* 2015 and are available upon request from co-author Alex Guenther. MOFLUX is part of the Ameriflux network and other observational data is available for download at <https://ameriflux.lbl.gov/sites/siteinfo/US-MOZ#BADM>. Satellite Ω HCHO is available publicly at https://cmr.earthdata.nasa.gov/search/concepts/C1626121562-GES_DISC.html.

8. Author contribution

EK and YW conceived the research idea. EK wrote the initial draft, conducted the simulations, and performed the analysis. EK and GF conducted model development. All authors contributed to the interpretation of the results and the preparation of the paper.

9. Competing interests

The authors declare that they have no conflict of interest.



References

- Arnth, A., Monson, R. K., Schurgers, G., Niinemets, Ü. and Palmer, P. I.: Why are estimates of global terrestrial isoprene emissions so similar (and why is this not so for monoterpenes)?, *Atmospheric Chemistry and Physics*, 8(16), 4605–4620, doi:10.5194/acp-8-4605-2008, 2008.
- Ball, T. and Berry, J.: A Simple Empirical Model of Stomatal Control. *Plant Physiology* 77(n. Supplement 4): 91, 1985.
- Bauer, S. E., Mishchenko, M. I., Lacis, A. A., Zhang, S., Perlwitz, J. and Metzger, S. M.: Do sulfate and nitrate coatings on mineral dust have important effects on radiative properties and climate modeling?, *Journal of Geophysical Research*, 112(D6), doi:10.1029/2005jd006977, 2007.
- Bauer, S. E., Tsigaridis, K., Faluvegi, G., Kelley, M., Lo, K. K., Miller, R. L., Nazarenko, L., Schmidt, G. A. and Wu, J.: Historical (1850–2014) Aerosol Evolution and Role on Climate Forcing Using the GISS ModelE2.1 Contribution to CMIP6, *Journal of Advances in Modeling Earth Systems*, 12(8), doi:10.1029/2019ms001978, 2020.
- Bauer, S. E., Wright, D. L., Koch, D., Lewis, E. R., McGraw, R., Chang, L.-S., Schwartz, S. E. and Ruedy, R.: MATRIX (Multiconfiguration Aerosol TRacker of mIXing state): an aerosol microphysical module for global atmospheric models, *Atmospheric Chemistry and Physics*, 8(20), 6003–6035, doi:10.5194/acp-8-6003-2008, 2008.
- Beguiría, S., Vicente-Serrano, S. M. and Angulo-Martínez, M.: A Multiscalar Global Drought Dataset: The SPEIbase: A New Gridded Product for the Analysis of Drought Variability and Impacts, *Bulletin of the American Meteorological Society*, 91(10), 1351–1356, doi:10.1175/2010bams2988.1, 2010.
- Beguiría, S., Vicente-Serrano, S. M., Reig, F. and Latorre, B.: Standardized precipitation evapotranspiration index (SPEI) revisited: parameter fitting, evapotranspiration models, tools, datasets and drought monitoring, *International Journal of Climatology*, 34(10), 3001–3023, doi:10.1002/joc.3887, 2014.
- Benjamin, M. T., Sudol, M., Bloch, L. and Winer, A. M.: Low-emitting urban forests: A taxonomic methodology for assigning isoprene and monoterpene emission rates, *Atmospheric Environment*, 30(9), 1437–1452, doi:10.1016/1352-2310(95)00439-4, 1996.
- Carlton, A. G., Wiedinmyer, C. and Kroll, J. H.: A review of Secondary Organic Aerosol (SOA) formation from isoprene, *Atmospheric Chemistry and Physics*, 9(14), 4987–5005, doi:10.5194/acp-9-4987-2009, 2009.
- Chance, K.: OMI/Aura Formaldehyde (HCHO) Total Column Daily L3 Weighted Mean Global 0.1deg Lat/Lon Grid V003, Greenbelt, MD, USA, Goddard Earth Sciences Data and Information Services Center (GES DISC), Accessed: [2021-04-07], 10.5067/Aura/OMI/DATA3010, 2019.
- Clapp, R. B. and Hornberger, G. M.: Empirical equations for some soil hydraulic properties, *Water Resources Research*, 14(4), 601–604, doi:10.1029/wr014i004p00601, 1978.



- 1003
1004 Dai, A.: Increasing drought under global warming in observations and models, *Nature Climate*
1005 *Change*, 3(1), 52–58, doi:10.1038/nclimate1633, 2013.
1006
1007 Emmerson, K. M., Palmer, P. I., Thatcher, M., Haverd, V. and Guenther, A. B.: Sensitivity of
1008 isoprene emissions to drought over south-eastern Australia: Integrating models and satellite
1009 observations of soil moisture, *Atmospheric Environment*, 209, 112–124,
1010 doi:10.1016/j.atmosenv.2019.04.038, 2019.
1011
1012 Farquhar, G. D. and von Caemmerer, S.: Modelling of Photosynthetic Response to
1013 Environmental Conditions. *Physiological Plant Ecology II: Water Relations and Carbon*
1014 *Assimilation*. O. L. Lange, P. S. Nobel, C. B. Osmond and H. Ziegler. Berlin, Heidelberg,
1015 Springer Berlin Heidelberg: 549–587, 1982.
1016 Geron, C., Guenther, A., Sharkey, T. and Arnts, R. R.: Temporal variability in basal isoprene
1017 emission factor, *Tree Physiology*, 20(12), 799–805, doi:10.1093/treephys/20.12.799, 2000.
1018
1019 Guenther, A., Karl, T., Harley, P., Wiedinmyer, C., Palmer, P. I. and Geron, C.: Estimates of
1020 global terrestrial isoprene emissions using MEGAN (Model of Emissions of Gases and Aerosols
1021 from Nature), *Atmospheric Chemistry and Physics*, 6(11), 3181–3210, doi:10.5194/acp-6-3181-
1022 2006, 2006.
1023
1024 Guenther, A. B., Jiang, X., Heald, C. L., Sakulyanontvittaya, T., Duhl, T., Emmons, L. K. and
1025 Wang, X.: The Model of Emissions of Gases and Aerosols from Nature version 2.1
1026 (MEGAN2.1): an extended and updated framework for modeling biogenic emissions,
1027 *Geoscientific Model Development*, 5(6), 1471–1492, doi:10.5194/gmd-5-1471-2012, 2012.
1028
1029 Henrot, A.-J., Stanelle, T., Schröder, S., Siegenthaler, C., Taraborrelli, D. and Schultz, M. G.:
1030 Implementation of the MEGAN (v2.1) biogenic emission model in the ECHAM6-HAMMOZ
1031 chemistry climate model, *Geoscientific Model Development*, 10(2), 903–926, doi:10.5194/gmd-
1032 10-903-2017, 2017.
1033
1034 Hoesly, R. M., Smith, S. J., Feng, L., Klimont, Z., Janssens-Maenhout, G., Pitkanen, T., Seibert,
1035 J. J., Vu, L., Andres, R. J., Bolt, R. M., Bond, T. C., Dawidowski, L., Kholod, N., Kurokawa, J.-
1036 I., Li, M., Liu, L., Lu, Z., Moura, M. C. P., O'Rourke, P. R. and Zhang, Q.: Historical (1750–
1037 2014) anthropogenic emissions of reactive gases and aerosols from the Community Emissions
1038 Data System (CEDS), *Geoscientific Model Development*, 11(1), 369–408, doi:10.5194/gmd-11-
1039 369-2018, 2018.
1040
1041 Huang, L., Mcgaughey, G., McDonald-Buller, E., Kimura, Y. and Allen, D. T.: Quantifying
1042 regional, seasonal and interannual contributions of environmental factors on isoprene and
1043 monoterpene emissions estimates over eastern Texas, *Atmospheric Environment*, 106, 120–128,
1044 doi:10.1016/j.atmosenv.2015.01.072, 2015.
1045
1046 Ito, G., Romanou, A., Kiang, N. Y., Faluvegi, G., Aleinov, I., Ruedy, R., Russell, G., Lerner, P.,
1047 Kelley, M. and Lo, K.: Global Carbon Cycle and Climate Feedbacks in the NASA GISS



- 1048 ModelE2.1, *Journal of Advances in Modeling Earth Systems*, 12(10),
1049 doi:10.1029/2019ms002030, 2020.
- 1050
- 1051 Jiang, X., Guenther, A., Potosnak, M., Geron, C., Seco, R., Karl, T., Kim, S., Gu, L. and
1052 Pallardy, S.: Isoprene emission response to drought and the impact on global atmospheric
1053 chemistry, *Atmospheric Environment*, 183, 69–83, doi:10.1016/j.atmosenv.2018.01.026, 2018.
- 1054
- 1055 Kaiser, J., Jacob, D. J., Zhu, L., Travis, K. R., Fisher, J. A., González Abad, G., Zhang, L.,
1056 Zhang, X., Fried, A., Crounse, J. D., St. Clair, J. M. and Wisthaler, A.: High-resolution inversion
1057 of OMI formaldehyde columns to quantify isoprene emission on ecosystem-relevant scales:
1058 application to the southeast US, *Atmospheric Chemistry and Physics*, 18(8), 5483–5497,
1059 doi:10.5194/acp-18-5483-2018, 2018.
- 1060
- 1061 Kelley, M., Schmidt, G. A., Nazarenko, L. S., Bauer, S. E., Ruedy, R., Russell, G. L., Ackerman,
1062 A. S., Aleinov, I., Bauer, M., Bleck, R., Canuto, V., Cesana, G., Cheng, Y., Clune, T. L., Cook,
1063 B. I., Cruz, C. A., Del Genio, A. D., Elsaesser, G. S., Faluvegi, G., Kiang, N. Y., Kim, D., Lacis,
1064 A. A., Leboisseries, A., Legrande, A. N., Lo, K. K., Marshall, J., Matthews, E. E., Mcdermid, S.,
1065 Mezuman, K., Miller, R. L., Murray, L. T., Oinas, V., Orbe, C., García-Pando, C. P., Perlwitz, J.
1066 P., Puma, M. J., Rind, D., Romanou, A., Shindell, D. T., Sun, S., Tausnev, N., Tsigaridis, K.,
1067 Tselioudis, G., Weng, E., Wu, J. and Yao, M.: GISS-E2.1: Configurations and Climatology,
1068 *Journal of Advances in Modeling Earth Systems*, 12(8), doi:10.1029/2019ms002025, 2020.
- 1069
- 1070 Kim, Y., Moorcroft, P. R., Aleinov, I., Puma, M. J. and Kiang, N. Y.: Variability of phenology
1071 and fluxes of water and carbon with observed and simulated soil moisture in the Ent Terrestrial
1072 Biosphere Model (Ent TBM version 1.0.1.0.0), *Geoscientific Model Development*, 8(12), 3837–
1073 3865, doi:10.5194/gmd-8-3837-2015, 2015.
- 1074
- 1075 Koch, D., Schmidt, G. A. and Field, C. V.: Sulfur, sea salt, and radionuclide aerosols in GISS
1076 ModelE, *Journal of Geophysical Research*, 111(D6), doi:10.1029/2004jd005550, 2006.
- 1077
- 1078 Koster, R. D., Guo, Z., Yang, R., Dirmeyer, P. A., Mitchell, K. and Puma, M. J.: On the Nature
1079 of Soil Moisture in Land Surface Models, *Journal of Climate*, 22(16), 4322–4335,
1080 doi:10.1175/2009jcli2832.1, 2009.
- 1081
- 1082 Li, W., Wang, Y., Flynn, J., Griffin, R. J., Guo, F. and Schnell, J. L.: Spatial Variation of Surface
1083 O₃ Responses to Drought Over the Contiguous United States During Summertime: Role of
1084 Precursor Emissions and Ozone Chemistry, *Journal of Geophysical Research: Atmospheres*,
1085 127(1), doi:10.1029/2021jd035607, 2022.
- 1086
- 1087 Loreto, F. and Sharkey, T. D.: A gas-exchange study of photosynthesis and isoprene emission in
1088 *Quercus rubra* L., *Planta*, 182(4), 523–531, doi:10.1007/bf02341027, 1990.
- 1089
- 1090 Miller, R. L., Cakmur, R. V., Perlwitz, J., Geogdzhayev, I. V., Ginoux, P., Koch, D., Kohfeld, K.
1091 E., Prigent, C., Ruedy, R., Schmidt, G. A. and Tegen, I.: Mineral dust aerosols in the NASA
1092 Goddard Institute for Space Sciences ModelE atmospheric general circulation model, *Journal of*
1093 *Geophysical Research*, 111(D6), doi:10.1029/2005jd005796, 2006.



- 1094
1095 Miller, R. L., Schmidt, G. A., Nazarenko, L. S., Bauer, S. E., Kelley, M., Ruedy, R., Russell, G.
1096 L., Ackerman, A. S., Aleinov, I., Bauer, M., Bleck, R., Canuto, V., Cesana, G., Cheng, Y.,
1097 Clune, T. L., Cook, B. I., Cruz, C. A., Del Genio, A. D., Elsaesser, G. S., Faluvegi, G., Kiang, N.
1098 Y., Kim, D., Lacis, A. A., Leboissetier, A., Legrande, A. N., Lo, K. K., Marshall, J., Matthews,
1099 E. E., Mcdermid, S., Mezuman, K., Murray, L. T., Oinas, V., Orbe, C., Pérez García-Pando, C.,
1100 Perlwitz, J. P., Puma, M. J., Rind, D., Romanou, A., Shindell, D. T., Sun, S., Tausnev, N.,
1101 Tsigaridis, K., Tselioudis, G., Weng, E., Wu, J. and Yao, M.: CMIP6 Historical Simulations
1102 (1850–2014) With GISS-E2.1, *Journal of Advances in Modeling Earth Systems*, 13(1),
1103 doi:10.1029/2019ms002034, 2021.
1104
1105 Müller, J.-F., Stavrakou, T., Wallens, S., De Smedt, I., Van Roozendaal, M., Potosnak, M. J.,
1106 Rinne, J., Munger, B., Goldstein, A. and Guenther, A. B.: Global isoprene emissions estimated
1107 using MEGAN, ECMWF analyses and a detailed canopy environment model, *Atmospheric*
1108 *Chemistry and Physics*, 8(5), 1329–1341, doi:10.5194/acp-8-1329-2008, 2008.
1109
1110 Monson, R. K., Weraduwa, S. M., Rosenkranz, M., Schnitzler, J.-P. and Sharkey, T. D.: Leaf
1111 isoprene emission as a trait that mediates the growth-defense tradeoff in the face of climate
1112 stress, *Oecologia*, 197(4), 885–902, doi:10.1007/s00442-020-04813-7, 2021.
1113
1114 Ochsner, T. E., Cosh, M. H., Cuenca, R. H., Dorigo, W. A., Draper, C. S., Hagimoto, Y., Kerr,
1115 Y. H., Larson, K. M., Njoku, E. G., Small, E. E. and Zreda, M.: State of the Art in Large-Scale
1116 Soil Moisture Monitoring, *Soil Science Society of America Journal*, 77(6), 1888–1919,
1117 doi:10.2136/sssaj2013.03.0093, 2013.
1118
1119 Opacka, B., Müller, J.-F., Stavrakou, T., Bauwens, M., Sindelarova, K., Markova, J. and
1120 Guenther, A. B.: Global and regional impacts of land cover changes on isoprene emissions
1121 derived from spaceborne data and the MEGAN model, *Atmospheric Chemistry and Physics*,
1122 21(11), 8413–8436, doi:10.5194/acp-21-8413-2021, 2021.
1123
1124 Pegoraro, E., Rey, A., Greenberg, J., Harley, P., Grace, J., Malhi, Y. and Guenther, A.: Effect of
1125 drought on isoprene emission rates from leaves of *Quercus virginiana* Mill., *Atmospheric*
1126 *Environment*, 38(36), 6149–6156, doi:10.1016/j.atmosenv.2004.07.028, 2004.
1127
1128 Potosnak, M. J., Lesturgeon, L., Pallardy, S. G., Hosman, K. P., Gu, L., Karl, T., Geron, C. and
1129 Guenther, A. B.: Observed and modeled ecosystem isoprene fluxes from an oak-dominated
1130 temperate forest and the influence of drought stress, *Atmospheric Environment*, 48, 314–322,
1131 doi:10.1016/j.atmosenv.2013.11.055, 2014.
1132
1133 Rasmusson, L. M., Gullström, M., Gunnarsson, P. C. B., George, R. and Björk, M.: Estimation
1134 of a whole plant Q10 to assess seagrass productivity during temperature shifts, *Scientific*
1135 *Reports*, 9(1), doi:10.1038/s41598-019-49184-z, 2019.
1136
1137 Rosenstiel, T. N., Potosnak, M. J., Griffin, K. L., Fall, R. and Monson, R. K.: Increased CO₂
1138 uncouples growth from isoprene emission in an agriforest ecosystem, *Nature*, 421(6920), 256–
1139 259, doi:10.1038/nature01312, 2003.



- 1140
1141 Schnell, J. L., Holmes, C. D., Jangam, A. and Prather, M. J.: Skill in forecasting extreme ozone
1142 pollution episodes with a global atmospheric chemistry model, *Atmospheric Chemistry and*
1143 *Physics*, 14(15), 7721–7739, doi:10.5194/acp-14-7721-2014, 2014.
- 1144
1145 Seco, R., Karl, T., Guenther, A., Hosman, K. P., Pallardy, S. G., Gu, L., Geron, C., Harley, P.
1146 and Kim, S.: Ecosystem-scale volatile organic compound fluxes during an extreme drought in a
1147 broadleaf temperate forest of the Missouri Ozarks (central USA), *Global Change Biology*,
1148 21(10), 3657–3674, doi:10.1111/gcb.12980, 2015.
- 1149
1150 Sharkey, T. D. and Singsaas, E. L.: Why plants emit isoprene, *Nature*, 374(6525), 769–769,
1151 doi:10.1038/374769a0, 1995.
- 1152
1153 Sharkey, T. D., Wiberley, A. E. and Donohue, A. R.: Isoprene Emission from Plants: Why and
1154 How, *Annals of Botany*, 101(1), 5–18, doi:10.1093/aob/mcm240, 2007.
- 1155
1156 Shindell, D. T., Pechony, O., Voulgarakis, A., Faluvegi, G., Nazarenko, L., Lamarque, J.-F.,
1157 Bowman, K., Milly, G., Kovari, B., Ruedy, R. and Schmidt, G. A.: Interactive ozone and
1158 methane chemistry in GISS-E2 historical and future climate simulations, *Atmospheric Chemistry*
1159 *and Physics*, 13(5), 2653–2689, doi:10.5194/acp-13-2653-2013, 2013.
- 1160
1161 Sindelarova, K., Granier, C., Bouarar, I., Guenther, A., Tilmes, S., Stavrakou, T., Müller, J.-F.,
1162 Kuhn, U., Stefani, P. and Knorr, W.: Global data set of biogenic VOC emissions calculated by
1163 the MEGAN model over the last 30 years, *Atmospheric Chemistry and Physics*, 14(17), 9317–
1164 9341, doi:10.5194/acp-14-9317-2014, 2014.
- 1165
1166 Singsaas, E. L. and Sharkey, T. D.: The effects of high temperature on isoprene synthesis in oak
1167 leaves, *Plant, Cell & Environment*, 23(7), 751–757, doi:10.1046/j.1365-3040.2000.00582.x,
1168 2000.
- 1169
1170 Skeie, R. B., Myhre, G., Hodnebrog, Ø., Cameron-Smith, P. J., Deushi, M., Hegglin, M. I.,
1171 Horowitz, L. W., Kramer, R. J., Michou, M., Mills, M. J., Olivié, D. J. L., Connor, F. M. O.,
1172 Paynter, D., Samset, B. H., Sellar, A., Shindell, D., Takemura, T., Tilmes, S. and Wu, T.:
1173 Historical total ozone radiative forcing derived from CMIP6 simulations, *npj Climate and*
1174 *Atmospheric Science*, 3(1), doi:10.1038/s41612-020-00131-0, 2020.
- 1175
1176 Sporre, M. K., Blichner, S. M., Karset, I. H. H., Makkonen, R. and Berntsen, T. K.: BVOC–
1177 aerosol–climate feedbacks investigated using NorESM, *Atmospheric Chemistry and Physics*,
1178 19(7), 4763–4782, doi:10.5194/acp-19-4763-2019, 2019.
- 1179
1180 Tawfik, A. B., Stöckli, R., Goldstein, A., Pressley, S. and Steiner, A. L.: Quantifying the
1181 contribution of environmental factors to isoprene flux interannual variability, *Atmospheric*
1182 *Environment*, 54, 216–224, doi:10.1016/j.atmosenv.2012.02.018, 2012.
- 1183



- 1184 Tsigaridis, K., Koch, D. and Menon, S.: Uncertainties and importance of sea spray composition
1185 on aerosol direct and indirect effects, *Journal of Geophysical Research: Atmospheres*, 118(1),
1186 220–235, doi:10.1029/2012jd018165, 2013.
- 1187
- 1188 Twomey, S.: Pollution and the planetary albedo, *Atmospheric Environment* (1967), 8(12), 1251–
1189 1256, doi:10.1016/0004-6981(74)90004-3, 1974.
- 1190
- 1191 Unger, N., Harper, K., Zheng, Y., Kiang, N. Y., Aleinov, I., Arneth, A., Schurgers, G.,
1192 Amelynck, C., Goldstein, A., Guenther, A., Heinesch, B., Hewitt, C. N., Karl, T., Laffineur, Q.,
1193 Langford, B., A. McKinney, K., Misztal, P., Potosnak, M., Rinne, J., Pressley, S., Schoon, N. and
1194 Serça, D.: Photosynthesis-dependent isoprene emission from leaf to planet in a global carbon-
1195 chemistry-climate model, *Atmospheric Chemistry and Physics*, 13(20), 10243–10269,
1196 doi:10.5194/acp-13-10243-2013, 2013.
- 1197
- 1198 Van Marle, M. J. E., Kloster, S., Magi, B. I., Marlon, J. R., Daniau, A.-L., Field, R. D., Arneth,
1199 A., Forrest, M., Hantson, S., Kehrwald, N. M., Knorr, W., Lasslop, G., Li, F., Mangeon, S., Yue,
1200 C., Kaiser, J. W. and Van Der Werf, G. R.: Historic global biomass burning emissions for
1201 CMIP6 (BB4CMIP) based on merging satellite observations with proxies and fire models (1750–
1202 2015), *Geoscientific Model Development*, 10(9), 3329–3357, doi:10.5194/gmd-10-3329-2017,
1203 2017.
- 1204
- 1205 Vicente-Serrano, S. M., Beguería, S. and López-Moreno, J. I.: A Multiscalar Drought Index
1206 Sensitive to Global Warming: The Standardized Precipitation Evapotranspiration Index, *Journal*
1207 *of Climate*, 23(7), 1696–1718, doi:10.1175/2009jcli2909.1, 2010.
- 1208
- 1209 Volkamer, R., San Martini, F., Molina, L. T., Salcedo, D., Jimenez, J. L. and Molina, M. J.: A
1210 missing sink for gas-phase glyoxal in Mexico City: Formation of secondary organic aerosol,
1211 *Geophysical Research Letters*, 34(19), doi:10.1029/2007gl030752, 2007.
- 1212
- 1213 Wang, P., Liu, Y., Dai, J., Fu, X., Wang, X., Guenther, A. and Wang, T.: Isoprene Emissions
1214 Response to Drought and the Impacts on Ozone and SOA in China, *Journal of Geophysical*
1215 *Research: Atmospheres*, 126(10), doi:10.1029/2020jd033263, 2021.
- 1216
- 1217 Wang, Y., Xie, Y., Dong, W., Ming, Y., Wang, J. and Shen, L.: Adverse effects of increasing
1218 drought on air quality via natural processes, *Atmospheric Chemistry and Physics*, 17(20),
1219 12827–12843, doi:10.5194/acp-17-12827-2017, 2017.
- 1220
- 1221 Wells, K. C., Millet, D. B., Payne, V. H., Deventer, M. J., Bates, K. H., De Gouw, J. A., Graus,
1222 M., Warneke, C., Wisthaler, A. and Fuentes, J. D.: Satellite isoprene retrievals constrain
1223 emissions and atmospheric oxidation, *Nature*, 585(7824), 225–233, doi:10.1038/s41586-020-
1224 2664-3, 2020.
- 1225
- 1226 Zhao, Z., Wang, Y., Qin, M., Hu, Y., Xie, Y. and Russell, A. G.: Drought Impacts on Secondary
1227 Organic Aerosol: A Case Study in the Southeast United States, *Environmental Science &*
1228 *Technology*, 53(1), 242–250, doi:10.1021/acs.est.8b04842, 2019.
- 1229



- 1230 Zhu, L., Jacob, D. J., Kim, P. S., Fisher, J. A., Yu, K., Travis, K. R., Mickley, L. J., Yantosca, R.
1231 M., Sulprizio, M. P., De Smedt, I., González Abad, G., Chance, K., Li, C., Ferrare, R., Fried, A.,
1232 Hair, J. W., Hanisco, T. F., Richter, D., Jo Scarino, A., Walega, J., Weibring, P. and Wolfe, G.
1233 M.: Observing atmospheric formaldehyde (HCHO) from space: validation and intercomparison
1234 of six retrievals from four satellites (OMI, GOME2A, GOME2B, OMPS) with SEAC4RS
1235 aircraft observations over the southeast US, *Atmospheric Chemistry and Physics*, 16(21), 13477–
1236 13490, doi:10.5194/acp-16-13477-2016, 2016.
- 1237
1238 Zhu, J., Penner, J. E., Lin, G., Zhou, C., Xu, L. and Zhuang, B.: Mechanism of SOA formation
1239 determines magnitude of radiative effects, *Proceedings of the National Academy of Sciences*,
1240 114(48), 12685–12690, doi:10.1073/pnas.1712273114, 2017.